MEMO 3-4-59E

NASA MEMO 3-4-59E

NASA

MEMORANDUM

EFFECTS OF NOSE RADIUS AND EXTREME COOLING ON BOUNDARY-LAYER TRANSITION FOR THREE SMOOTH 15°-CONE-CYLINDERS IN FREE FLIGHT AT MACH NUMBERS TO 8.50

By M. J. Krasnican and L. Rabb

Lewis Research Center
Cleveland, Ohio

NATIONAL AERONAUTICS AND SPACE ADMINISTRATION

WASHINGTON

March 1959

NATIONAL AERONAUTICS AND SPACE ADMINISTRATION

MEMORANDUM 3-4-59E

EFFECTS OF NOSE RADIUS AND EXTREME COOLING ON BOUNDARY-LAYER TRANSITION FOR THREE SMOOTH 15°-CONE-CYLINDERS IN FREE FLIGHT AT MACH NUMBERS TO 8.50*

By M. J. Krasnican and L. Rabb

SUMMARY

Three highly polished 15°-included-angle cone-cylinders with hemispherical tips of several diameters (2, 3, and 4 in.) have been flown in order to obtain boundary-layer transition data at very low wall to local stream temperature ratios, and heat-transfer data. All surfaces had a 2-microinch average roughness height.

Laminar flow existed over the entire hemispherical nose of the 2- and 3-inch-tip-diameter models throughout the complete flight history. Extreme cooling to wall to local stream temperature ratios at the sonic point as low as 0.20 did not cause transition on the nose for diameters as large as 3 inches. However, extreme cooling did cause early transition on the 4-inch model where it appears probable that transition occurred forward of the 45° station at a wall to local stream temperature ratio of about 0.26.

Variations in tip diameter influenced transition downstream of the nose under conditions of extreme cooling. The 2-inch-tip model was laminar at all cone-cylinder stations at temperature ratios as low as 0.32 whereas the 3- and 4-inch-tip models were turbulent at the same local flow conditions but at higher wall to local temperature ratios. Transition on the cone and cylinder of the 3- and 4-inch-tip bodies appeared to be sensitive to local Mach number, and occurred at higher local temperature ratios when values of local Mach number were higher. Increasing the nose diameter from 2 to 3 inches significantly changed the local flow conditions for which laminar flow existed on the cone-cylinder afterbody. However, a further increase in tip size to a 4-inch diameter had no discernable effect on the local flow conditions at transition.

*Title, Unclassified.

The transition results of the 3- and 4-inch-nose-diameter smooth bodies are similar to those observed on a 7/8-inch-nose-diameter body with roughened surfaces. Turbulent boundary layers resulted in both cases at very low wall to local stream temperature ratios.

Both laminar and turbulent heat-transfer data were in good agreement with theoretical Stanton numbers when heat-transfer reduction due to tip blunting was considered.

INTRODUCTION

The NASA Lewis Research Center has employed the free-flight, air-launch method for studying a number of boundary-layer transition and heat-transfer phenomena. Among the problems investigated has been the favorable effect of small amounts of tip bluntness in raising the permissible skin temperature for a given boundary-layer transition Reynolds number (refs. 1 and 2). Also examined has been the effect of surface roughness and extreme cooling on transition (ref. 3). It has been shown that surface cooling can delay transition and lead to long runs of laminar flow (refs. 1 and 2). However, the data of reference 4 shows that excessive cooling can lead to low transition Reynolds numbers. In contrast to the favorable effects of moderate tip blunting on boundary-layer transition, large amounts of tip bluntness in the presence of extreme cooling can lead to low transition Reynolds numbers. This phenomenon is discussed in reference 5 where transition was correlated on hemispherical-nosed bodies and in reference 4 where transition was observed on cone-cylinder bodies under conditions of extreme cooling. The question naturally arises as to how much blunting in the presence of extreme cooling can be tolerated on slender models without causing transition. In order to investigate this problem, three smooth (2 microin. average roughness height) 15°-included-angle cone-cylinders with hemispherical tips of several diameters (2, 3, and 4 in.) were flown. All of the vehicles were launched from a jet aircraft at high altitude and were accelerated to high Mach numbers by two stages of solid-propellant rocket. Data on boundary-layer transition and heat transfer from these flight tests are presented herein.

MODEL AND INSTRUMENTATION

Sketches of the three models flown are shown in figure 1. A photograph of a typical test body (model A) and booster assembly is shown in figure 2. Photographs of model B and C nose cones are shown in figures 3(a) and (b), respectively. Table I lists physical data on the test bodies. These test bodies are similar except for the amount of tip bluntness, and will be designated throughout the report as models A, B, and C with hemispherical tip diameters of 2, 3, and 4 inches, respectively.

The model forebody in each case consisted of a 15°-included-angle cone with a 6-inch-diameter base. All test bodies had nickel tips as indicated in figure 1. The cone skin was made of 0.060-inch (nominal) nickel for model A, and Inconel for models B and C. The actual skin thicknesses are shown on figure 1 for each station. The preceding conical forebodies were attached to 0.032-inch (nominal) Inconel cylinders. A lava (Alsimag) ring served as thermal and electrical insulation between the instrumented cone-cylinder and the rocket afterbody, and enabled the afterbody skin to function as the telemeter antenna. The sustainer rocket (T-55) occupied the volume aft of the lava ring. The rear of the test body consisted of a 10°-half-angle flared skirt which was treated with a coating of "thermo-clad" insulation to protect the skirt from severe aerodynamic heating. The nose cone and instrumented portion of the cylinder of each model was highly polished to a surface finish of the order of 2-microinches average roughness height. The aft portion of the cylinder (uninstrumented) was chemically blackened to increase its emissivity and thus reduce peak skin temperatures on its surface.

Each model was instrumented with thermocouples for measuring skin temperatures, two axial accelerometers and a cone pressure tap. In addition, models A and C had stagnation pressure taps, model B had a cylinder pressure tap, and model C had two lateral accelerometers. The location of the skin-temperature thermocouples as well as the ranges of all instruments used are shown in figure 1. On all models, thermocouples located in the nose were integral parts of Inconel slugs which were inserted through (press fit) holes, and were welded at the outer skin surface and polished smooth. Slug thickness (depth) was 1/8 inch on models A and B, while it was 3/8 inch on model C. The thin wall thermocouples were installed as follows: Two adjacent holes were drilled through the skin. Chromel-Alumel wires were inserted from within and a junction was formed by welding on the skin exterior; this region was ground and polished smooth.

The acceleration and pressure measurements were continuous while skin-temperature thermocouple measurements were commutated so that each temperature was recorded at intervals of about 0.2 second. All of the thermocouples were Chromel-Alumel. A built-in calibration system permitted a cyclic temperature calibration (0, 1/2, full scale) to be recorded about every 0.2 second.

A radio telemeter transmitter was used to send data to ground receiving stations. This telemeter assembly was housed in the volume enclosed by the polished, instrumented cone-cylinder.

The models were propelled by a T-64 (Recruit) rocket booster, and by a T-55 sustainer rocket carried within the cylindrical and flared parts of the model. Table II lists data on these rockets. High

expansion-ratio nozzles were used with the T-55 rockets. The booster assembly and sustainer rocket were locked together by a frangible disk coupling. Separation of the two stages occurred upon firing of the T-55 sustainer rocket.

PROCEDURE

Each model was air-launched in level flight from an F2H-2B airplane at high altitude and allowed to fall in a zero-lift trajectory. The test vehicles were accelerated to high speeds by booster and sustainer rockets which were energized by time-delay squibs as the models left the launch aircraft. All the data were transmitted to NASA ground receiver stations at Wallops Island, Virginia. These models were tracked to a limited extent by ground radar and phototheodolite equipment. This procedure is identical to that discussed in references 1 and 2.

The method of data reduction is similar to that described in reference 6. The data presented herein are in terms of local flow properties. These local conditions on the cone-cylinder are based on the method of reference 7 and on calculated static-pressure distribution for cone-cylinder bodies of revolution given in reference 8. The local total pressure at all stations was computed from the free-stream Mach number and the normal shock relations given in reference 9.

Local flow properties on the blunt nose were based on the modified Newtonian pressure distribution and a power-law variation of viscosity with temperature. The exponent was assumed equal to 0.76. The local specific heat ratio γ was based on reference 10. The calculated variation of Reynolds number at several angular positions along the nose is presented in figure 4.

Data reduction at or near peak temperature was difficult because the wall-temperature time derivatives were nearly zero. Also, the difference between the adiabatic wall temperature and local wall temperature was approaching zero. In some cases possible transition points near peak temperatures were indeterminate because of the above effect.

Uncertainties in the instrumentation on the blunt nose of model C concern the depth (ε) of the thermocouples from the outer surface (shown in the following sketch).

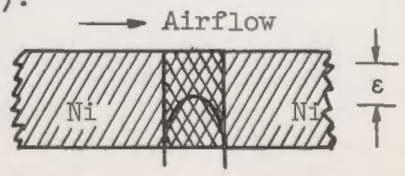

Inconel insert Thermocouple leads

The measured heating rates on the nose were extremely sensitive to any changes in ε because Inconel inserts were inadvertently installed in the nickel nose. Variation of ε from 0.015 to 0.090 inch was found to change the calculated heating rates from laminar to turbulent values. Transition was, therefore, determined by an examination of the temperature-time histories of the $22\frac{1}{2}^{\circ}$ and 45° stations of model C.

HEAT-TRANSFER AND BOUNDARY-LAYER TRANSITION RESULTS

The primary data and the local flow conditions are discussed in appendix A. Appendix B treats the interpretation of transition data.

Nondimensional heat-transfer coefficients in the form of Stanton numbers were calculated from measured skin-temperature - time histories and are shown in figure 5. Also shown are the theoretical Stanton numbers St for both laminar and turbulent flow. The theoretical Stanton numbers were obtained from references 11 to 19 for the known local flow conditions. In general, the data are in reasonably good agreement with the theoretical Stanton numbers. When transition occurred, transition points were usually well defined and were considered to be the initial points of deviation from the laminar or turbulent values. These points are indicated on figure 5.

A brief summary of the transition results encountered in each flight is as follows:

Model A - The boundary layer remained laminar on model A during the entire flight. Typical Stanton number time histories are shown in figure 5(a). One exception might be made at 1.2 seconds where the curve for station 10 shows a sharp increase in the Stanton numbers, followed by a decreasing trend. This station was located 180° from the mainline of instrumentation shown in figure 1(a).

Model B - Boundary-layer transition points were observed on model B at all stations aft of the nose. Figure 5(b) shows good agreement between the present data and the theoretical laminar Stanton numbers at station 2 (45° from the stagnation point) during most of the flight. Typical Stanton number time histories for model B are shown in figure 5(b).

Model C - Stanton numbers of model C indicated that transition at most stations may have occurred at three distinct times. The boundary layer changed from laminar to turbulent, turbulent to laminar, and back to turbulent. For example, figure 5(c) shows transition points at 1.0, 5.4, and 6.9 seconds for station 5. This suggests that the transition point of model C moved forward, aft, and then forward again. These changes depended on the local flow conditions and will be discussed later. The second movement of the transition point on the cone began at 5.0

seconds. Obviously, the boundary layer at $\theta = 45^{\circ}$ must also have been laminar at 5.0 seconds. (Symbols are defined in appendix C.) It is unlikely that turbulent flow could have existed on the nose and laminar flow on the cone. Transition on the nose must, therefore, have moved past the $\theta = 45^{\circ}$ station at some time earlier than 5.0 seconds. Temperature measurements on the nose at times greater than 3.4 seconds were not considered reliable. However, temperature fluctuations at $\theta = 45^{\circ}$ at times greater than 2 seconds may indicate some movement of the transition point at this time. Transition was, therefore, assumed at $\theta = 45^{\circ}$ at approximately 2.2 seconds. The third transition movement of model C occurred near peak temperature. It was very difficult to evaluate the Stanton numbers at this time because of the inherent problem at peak temperatures mentioned in the PROCEDURE section. The third transition was positively observed at only two stations (5 and 8). Since the transition point was moving forward on the body, it may have moved past the forward stations (4 and 3) at some time greater than that observed for station 5. For this case, transition would most certainly have been masked by the small temperature slopes at peak temperature.

The various flow parameters at each transition point for all three models are summarized in table III. In the following discussion, the transition data on the nose and cone-cylinder afterbody are treated separately.

Boundary-layer transition on the nose. - Moderate amounts of tip bluntness can lead to long laminar runs under extreme cooling (ref. 7). However, increased bluntness under the same conditions of cooling may initiate early transition. This has been found in tests at the NASA Langley, Ames, and Lewis Research Centers. It is desirable, therefore, to know what parameters influence transition on highly cooled blunt bodies. An interesting correlation of blunt-body transition results is given in reference 5 where it is shown that a critical correlation parameter does exist. The present data are compared with this correlation in figure 6. Excellent agreement between the present transition data and the correlation curve of reference 5 is noted. The open symbols of figure 6 are for laminar flow conditions and the solid symbols are for turbulent conditions. An analysis of the temperature data at $\theta = 45^{\circ}$ as compared with the data at $\theta = 22.5^{\circ}$ on model C indicated that turbulent heating rates began at approximately 1.35 seconds. At this time the ratio of wall to total enthalpy was 0.21 and the value of the correlation parameter of reference 5 was 109.

The correlation parameter of reference 5 is a useful tool for predicting transition on a highly cooled blunt body. However, the parameter is rather difficult to evaluate. In terms of an engineering approximation, a more convenient method of presenting transition results for blunt bodies is shown in figure 7 where a new correlation curve based on data in reference 5 is presented. The parameters of interest are the ratio

of wall to local stream temperature at the sonic points on the nose $(t_w/t_l)_{45}$ and the ratio of the local Reynolds number at the sonic point to the Mach number ahead of the bow shock (Re_{45}/M_0). These parameters are easy to evaluate and appear to correlate all the hemisphere data used in the correlation of reference 5. The authors recognize that the parameters of figure 7 are entirely empirical and no explanation is offered to tell why the correlation is valid. It is further emphasized that the data are confined to hemispherical bodies. The gas properties used for the correlation parameters of figure 7 are for real gases and the Reynolds number is based on the wetted distance from the stagnation point to the sonic point on the nose. The curve presented as figure 4 was found useful in evaluating the Reynolds number at the sonic point.

Figure 7 also presents the data for the three blunted cone-cylinder models of this report. Time histories of each model are similar, but the range of Re_{45}/M_0 is due to differences in the reference length at the sonic point. Data are shown for tip diameters of 7/8 inch (ref. 3), 2, 3, and 4 inches. Thermocouples at the sonic point ($\theta = 45^\circ$) were not installed on the 2-inch model nor on the 7/8-inch-tip model of reference 3. Consequently, the data of these two models are based on estimated wall temperatures at the sonic point. The data shown for the 3- and 4-inch-tip-diameter models are based on measured wall temperatures. However, the thermocouple at $\theta = 45^\circ$ on the 4-inch model ceased functioning at approximately 4 seconds, and estimated values were used thereafter.

Laminar flow was observed on the afterbody of the 2-inch-tip body (fig. 5(a)) and also on the 7/8-inch-tip body (ref. 3). Consequently, the data for both models as presented are assumed to be laminar. The data for the 3-inch model is also laminar (fig. 5(b)). However, the boundary layer on the cone afterbody was turbulent even though the tip was laminar. This case will be discussed later. Transition occurred twice on the nose of model C. At the first time of transition, the flow went from laminar to turbulent at $(t_w/t_l)_{45} = 0.27$ and Re_{45}/M_0 of 1.3×10^5. The boundary layer was believed to have changed back to laminar flow at approximately 2.2 seconds. The local conditions were: $(t_w/t_l)_{45} = 0.27$ and $Re_{45}/M_0 = 1.1\times10^5$. These values are listed in table III, but are not shown in figure 7.

The above discussion concerning model C must be qualified by the previously mentioned uncertainty in the thermocouple instrumentation. However, it can be said that the present data do not contradict other results on highly cooled blunt bodies. Laminar flow can be maintained on the nose of highly cooled blunt bodies provided that for the particular stream conditions, tip diameter is not so large as to enter the turbulent region defined in figure 7. For the flight conditions encountered herein, a limiting tip size of about 3 inches would be marginal if

laminar flow were to be maintained throughout the flight. For the 3-inch tip, laminar flow existed with $(t_w/t_l)_{45}$ of 0.20 and Re_{45}/M_O of 0.88×10^5.

Boundary-layer transition on cone-cylinder afterbody. - The previous discussion suggests that there are some limits on the amount of tip bluntness and cooling which a slender body can tolerate and still maintain laminar flow on the blunt nose. Another question which comes to mind is whether the tip size influences the boundary layer downstream even though the tip itself is laminar. The answer apparently is yes. The transition results of this report show that in some cases although the boundary layer on the 3- and 4-inch tips was laminar, the boundary layer downstream of the tip was turbulent. In particular, transition was observed on the cone-cylinder of models B and C when the boundary layer was subjected to extreme cooling. These findings were similar to the "transition reversal" results discussed in reference 4. The so-called "reversal" phenomenon refers to the fact that moderate cooling tends to promote larger runs of laminar flow whereas excessive cooling under certain conditions can cause the boundary layer to become turbulent. This is illustrated in figure 8 and in the summary of data in figure 9(a).

The wall to local stream temperature ratio (t_w/t_l) and local Reynolds number (Re_l) at each cone and cylinder station for all three models are shown in figure 8. Open symbols are used for laminar flow conditions and closed symbols represent turbulent flow conditions; arrows indicate increasing time. The data presented in figure 8(a) for the 2-inch tip diameter shows that all cone and cylinder stations are laminar. Minimum t_w/t_l on the cone ranged from 0.35 at station 2 to 0.32 at station 6. Lowest values of t_w/t_l on the cylinder were slightly higher and were approximately 0.43 at all cylinder stations.

A summary of the transition results of figures 8(b) and (c) is presented in figure 9(a). Some additional points from model A and the 7/8-inch-tip-diameter body of reference 3 are also shown in figure 9(a). These points are minimum t_w/t_l values for laminar boundary layers. Again, open symbols represent laminar flow conditions and closed symbols denote transition points. The local conditions shown in figure 9(a) for the 3- and 4-inch-diameter models of this report have also been tabulated in table III. Arrows indicate which way the local parameters are changing with increasing time. Finally, the smooth body transition results of reference 4 are shown as a solid line.

In general, the data in figure 9(a) show some interesting effects on afterbody transition results which may be attributed to tip size in the presence of extreme cooling. Three regions are defined in figure 9(a) and

are illustrated in the following sketch:

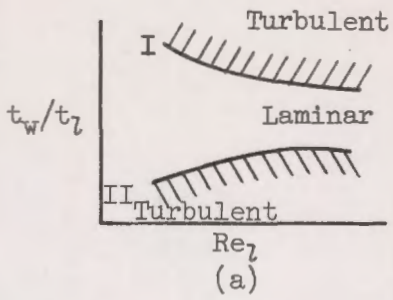

(a)

The turbulent region bounded by curve I is from the summary of sharp-tip, smooth-body transition results presented in reference 3. The turbulent region bounded by curve II is defined by the present data of models B and C. Reference to figure 9(a) shows that laminar-boundary layers were observed on the cone and cylinder of model A and also on the 7/8-inch-tip model of reference 3 at temperature ratios well below the transition values of models B and C (below curve II). Thus, while extreme cooling adversely affected the 3- and 4-inch models, it had no effect on the 7/8- and 2-inch models at t_w/t_l as low as 0.32 on the cone and 0.43 on the cylinder. In the case of model C, the turbulent region below curve II (sketch (a)) was defined twice during the flight. In the first case, the temperature ratios were decreasing, and in the second case the temperature ratios were increasing (fig. 9(a)). Some scatter is evident in figure 9(a) but this may be a Mach number effect. For example, a study of cone station 3 and table III indicates that t_w/t_l at the first transition was 0.67 at a Re_l of 1.0×10^6 while at the second transition time a slightly higher t_w/t_l of 0.79 occurred at the same Reynolds number. The corresponding local Mach number changed from 2.20 to 2.84. Another indication of a possible Mach number effect is noted when the t_w/t_l at transition is compared on the cone and cylinder. The cylinder values are generally greater than cone values and occur at higher Mach numbers. This possible Mach number effect is further illustrated in figure 9(b) where all of the transition data listed in table III have been plotted. In general, transition occurred at higher t_w/t_l when the local Mach number increased. The preceding discussion must be qualified by the unknown effects of local pressure gradient around the cone-cylinder junction, and possible Reynolds number per foot and roughness effects.

Also shown in figure 9(b) are the transition results of the rough surface model with a 7/8-inch tip (ref. 3) and the stability curve of reference 20. The results of reference 3 are similar to the present findings of models B and C, also shown in figure 9(b). Since the transition results of reference 3 were due to surface roughness and not to tip size, transition in the presence of extreme cooling can be caused by

either roughness or excessive bluntness. What determines excessive bluntness is not clear. However, for the flight trajectories of the present models (A, B, and C), tip diameters between 2 and 3 inches appear to be critical for transition on the afterbody in the presence of extreme cooling. Changes in tip size from 3 to 4 inches (diam.) had no additional effect on transition results.

The location of some thermocouples 180° from the mainline of instrumentation is shown in figure 1. Table III lists the transition points of these stations. A total of 5 transition points on the opposite sides were recorded. These points are plotted in figure 9. In general, these points agree with the data from the mainline of instrumentation. Two points, however, show disagreement with the majority of the data. The two points are: a cone station of model B (station 10) and a cylinder station on model C (station 10). The transition results of these two stations may indicate the degree of reproducibility which can be expected in transition data under these conditions.

SUMMARY OF RESULTS

Three smooth 15°-cone-cylinders with nose diameters of 2, 3, and 4 inches have been flown in order to evaluate the effects of varying degrees of bluntness on boundary-layer transition under conditions of extreme cooling. The results have been discussed keeping in mind blunt-body transition and the effects of nose bluntness on slender body transition. The following results were obtained:

1. Laminar flow existed over the entire hemispherical nose of the 2- and 3-inch-tip-diameter models during the complete time history of each flight. Extreme cooling to local wall to stream temperature ratios at the sonic point as low as 0.20 did not cause transition on the nose for diameters as large as 3 inches. However, extreme cooling did cause early transition on the 4-inch-nose-diameter model where it appears probable that transition occurred forward of the 45° station on the nose at a local wall to stream temperature ratio of 0.26. Uncertainties in the instrumentation on the nose of the 4-inch model prevented positive conclusions regarding transition on the nose.

2. The present data show that variations in the nose diameter can influence transition downstream on the model. The 2-inch-tip model was laminar at all stations at local temperature ratios as low as 0.20 whereas the 3- and 4-inch models were turbulent at the same local flow conditions but at higher temperature ratios.

3. For the flight trajectories of this report it was found that increasing nose diameters from 2 to 3 inches materially changes the location of transition on the cone-cylinder surfaces of the models. However, a further increase in tip size to 4-inch diameter had no effect on cone-cylinder transition results.

4. Transition on the cone and cylinder of the 3- and 4-inch-tip-diameter bodies appeared to be sensitive to local Mach number, and apparently occurred at higher local temperature ratios when values of local Mach numbers were higher.

5. Transition results of the 3- and 4-inch-nose-diameter bodies are similar to those observed on 7/8-inch-nose-diameter body with roughened surface. Turbulent boundary layers resulted in both cases when very low local stream temperature ratios within the so-called "reversal region" were reached.

Lewis Research Center
National Aeronautics and Space Administration
Cleveland, Ohio, December 3, 1958

APPENDIX A

PRIMARY DATA AND LOCAL CONDITIONS

Primary Data

The primary data for all three models are presented in figures 10 to 18. This information is given as time histories. It should be noted that models A, B, and C encountered somewhat similar flight conditions during the accelerating phases of the flights.

The first-stage (booster) accelerations shown in figure 11 ranged from about 70 to 140 g's. Models B and C decelerated normally after first-stage burning while model A apparently had premature sustainer ignition which resulted in model damage and telemeter signal failure shortly thereafter. Model B sustainer had a high initial acceleration during ignition and then operated normally for about 0.2 seconds at which time structural or telemeter failure occurred.

Data were recorded during the boost phase and during the complete coasting flight for model C. The sustainer stage of this model had a nominal acceleration of about 45 g's during burning. At about 8 seconds, the body experienced severe lateral accelerations as indicated in figure 11 (model C). In addition, figure 16 shows that model C, after 8 seconds, was at considerable angle of attack. Therefore, data beyond 7.5 seconds was not considered in the heat-transfer analysis.

The free-stream Mach numbers are shown in figure 12. Maximum values for models A, B, and C were 6.34, 6.76, and 8.50, respectively. The corresponding maximum free-stream Reynolds numbers per foot for each model were 11.22×10^6, 15.95×10^6, and 19.70×10^6, as shown in figure 13. A peak free-stream total temperature of 5325° R was calculated for model C.

Local Conditions (Stream)

The variation of measured total pressure during the flights of models A and C is shown in figure 14. Time histories of measured cone static pressure for all models is given in figure 15. In the case of model C note the severe oscillations in measured cone pressure after 8 seconds, and its correspondence with the large lateral accelerations experienced by the vehicle (fig. 11). Cylinder static pressure was measured on model B only (fig. 17). Local stream conditions were based on calculated static-pressure distributions over the cone-cylinders. In addition, all local stream conditions were corrected for tip bluntness by the method of reference 7.

Local stream Reynolds number per foot Re_l and Mach number M_l are presented as time histories in figure 19 for models A, B, and C. The values Re_l and M_l are substantially less than free-stream values because of nose tip blunting. Local conditions at minimum observed temperature ratios are shown in the following table:

Local Conditions at Minimum Observed Temperature Ratios

Location	Station	t_w/t_l	M_l	Re_l	Boundary layer
Model A (2-in.-diam. tip)					
Cone	6	0.32	2.71	3.10×10^6	Laminar
Cylinder	7	.44	3.45	2.05	↓
Cylinder	8	.42	3.41	2.68	
Cylinder	9	.42	3.39	3.39	
Model B (3-in.-diam. tip)					
Cone	6	0.37	2.70	2.71×10^6	Turbulent
Cylinder	7	.51	3.43	1.92	↓
Cylinder	8	.50	3.39	2.64	
Cylinder	9	.48	3.38	3.39	
Model C (4-in.-diam. tip)					
Cone	5	0.40	2.69	1.88×10^6	Turbulent
Cylinder	7	.49	3.24	2.07	↓
Cylinder	8	.49	3.22	2.92	

The variation of wall to local stream temperature ratio with local Mach number for the cone and cylinder stations of models A, B, and C, are shown in figures 20(a), (b), and (c), respectively, together with the theoretical infinite stability limits of reference 20.

Local Conditions (Wall)

Time histories of measured wall temperatures are presented in figure 18. Peak wall temperatures for models A and B were much lower than those of model C due to the shorter recorded flight times involved. In the case of models A and B, the skin thicknesses used in the tip heat-transfer calculations were those of the thermocouple slugs, namely, 1/8-inch. Since lateral temperature distribution on the nose tip was not measured, a one-dimensional calculation for heat flux into the tip was used. In the case of model C, in addition to lateral conduction errors, additional error existed due to the uncertainty in the exact depth of the

tip thermocouple junctions from the surface. These errors in the absolute magnitude of the calculated heat flux on the tip, however, are not considered large enough to prevent determination of whether the boundary layer on the tip was laminar or turbulent.

Values of wall to local stream temperature ratio, t_w/t_l, ranged from a minimum of 0.20 at the 45° stations of model B (fig. 7) to a maximum of 2.06 at station 7 of model C (fig. 8(c)). The local stream temperature t_l at each station was also corrected for tip bluntness effects by the method of reference 7.

APPENDIX B

INTERPRETATION OF TRANSITION DATA

When transition occurs at essentially the same time at all stations, it is not clear whether all points should be considered as valid transition points, or only the data of the most forward station. The purpose of this appendix is to justify our contention that for Model B, and for the data of Model C at $t = 1$ second, all points are valid transition points.

When transition takes place at different stations on the body at nearly identical times, it might be assumed that transition occurred when conditions at the most forward station were such as to cause transition and that the rear stations merely respond to the upstream disturbances. For this case (case I) the transition points on the aft stations could not be considered as true transition points. This suggests that the forward stations approach the critical flow conditions before the rear stations. Consequently, a specific correlation curve is implied. For example, consider transition to be affected by only two parameters: (a) t_w/t_l and (b) Reynolds number. The temperature gradient along the body is also negligible. Case I would then suggest a correlation curve with a negative slope (sketch (a)).

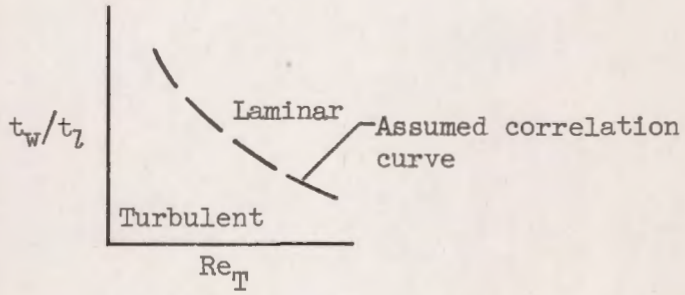

(a)

If stations 3, 4, and 5 were placed on such a plot (sketch (a)), then station 3 would cross the correlation curve first at point A (sketch (b)). The conditions at station 3 would then have determined the state of the boundary layer at the rear stations so that only the transition at point A would be valid.

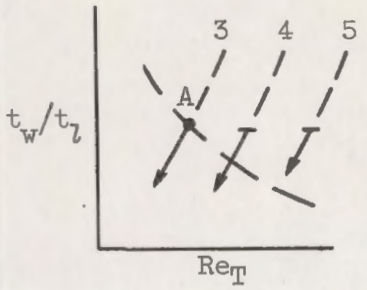

(b)

However, data reported in reference 4 and the present data of Model C at approximately 5.0 seconds show that the correlation curve (in the so-called reversal region) has a slope which is positive (see sketch (c)).

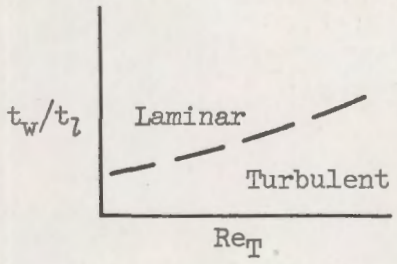

(c)

If the time histories of stations 3, 4, and 5 are inserted near 1.0 second on sketch (c), a situation as pictured in sketch (d) results.

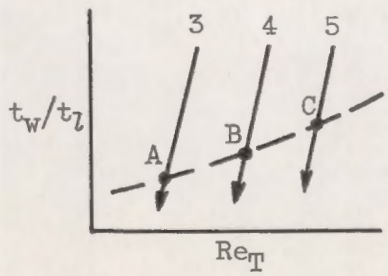

(d)

For the above case (case II), shown in sketch (d), transition would occur first at point C and move forward to point A a short time later. If the slope of the correlation curve were nearly zero, then the movement of the transition point forward would be very rapid. Consequently, some transition points could appear simultaneously within the sensitivity of the instrumentation.

An additional point which should be stressed is that transition is assumed to move continuously on the body. Since the boundary layer was initially laminar during the present flight tests, the first appearance of transition is assumed to be a continuous movement from the rear stations forward. Therefore all stations are considered to have valid transition points and have been tabulated in table III.

APPENDIX C

SYMBOLS

$a_{L,R}$	resultant lateral acceleration, g's
a_N	axial acceleration, g's
h_w/h_o	wall to total enthalpy ratio
M	Mach number
P_{ob}	total pressure behind shock, lb/sq in. abs
p	static pressure, lb/sq in. abs
Re	Reynolds number
Re_l^*/M_e	correlation parameter of ref. 4
St	Stanton number
t	static temperature, ^oR
z	altitude, ft
α	circumferential angle about longitudinal axis, deg
γ	specific heat ratio
ε	depth of thermocouple from outer surface of skin, in.
θ	angle from stagnation point to instrumentation on the hemispherical tip

Subscripts:

c	cone surface
cyl	cylinder surface
l	local condition just outside of boundary layer
T	transition
w	body surface condition

0 free-stream conditions ahead of shock

45 at 45° nose station

REFERENCES

1. Disher, John H., and Rabb, Leonard: Observation of Laminar Flow on a Blunted 15° Cone-Cylinder in Free Flight at High Reynolds Numbers and Free-Stream Mach Numbers to 8.17. NACA RM E56G23, 1956.

2. Rabb, Leonard, and Krasnican, Milan J.: Observation of Laminar Flow on an Air-Launched 15° Cone-Cylinder at Local Reynolds Numbers to 50×10^6 at Peak Mach Number of 6.75. NACA RM E56L03, 1957.

3. Rabb, Leonard, and Krasnican, Milan J.: Effects of Surface Roughness and Extreme Cooling on Boundary-Layer Transition for 15° Cone-Cylinder in Free Flight at Mach Numbers to 7.6. NACA RM E57K19, 1958.

4. Jack, John R., Wisniewski, Richard J., and Diaconis, N. S.: Effects of Extreme Surface Cooling on Boundary-Layer Transition. NACA TN 4094, 1957.

5. Wisniewski, Richard J.: A Note on a Correlation of Boundary-Layer Transition Results on Highly Cooled Blunt Bodies. NASA MEMO 10-8-58E, 1958.

6. Rabb, Leonard, and Simpkinson, Scott H.: Free-Flight Heat-Transfer Measurements on Two 20°-Cone-Cylinders at Mach Numbers from 1.3 to 4.9. NACA RM E55F27, 1955.

7. Moeckel, W. E.: Some Effects of Bluntness on Boundary-Layer Transition and Heat Transfer at Supersonic Speeds. NACA Rep. 1312, 1957. (Supersedes NACA TN 3653.)

8. Clippinger, R. F., Giese, J. H., and Carter, W. C.: Tables of Supersonic Flows about Cone Cylinders. I - Surface Data. Rep. No. 729, Ballistic Res. Labs., Aberdeen Proving Ground (Md.), July 1950.

9. Ames Research Staff: Equations, Tables, and Charts for Compressible Flow. NACA Rep. 1135, 1953. (Supersedes NACA TN 1428.)

10. Moeckel, W. E.: Oblique-Shock Relations at Hypersonic Speeds for Air in Chemical Equilibrium. NACA TN 3895, 1957.

11. Van Driest, E. R.: Investigation of Laminar Boundary Layer in Compressible Fluids Using the Crocco Method. NACA TN 2597, 1952.

12. Van Driest, E. R.: Turbulent Boundary Layer on a Cone in a Supersonic Flow at Zero Angle of Attack. Jour. Aero. Sci., vol. 19, no. 1, Jan. 1952, pp. 55-57; 72.

13. Cohen, Clarence B., and Reshotko, Eli: The Compressible Laminar Boundary Layer with Heat Transfer and Arbitrary Pressure Gradient. NACA Rep. 1294, 1956. (Supersedes NACA TN 3326.)

14. Reshotko, Eli: Simplified Method for Estimating Compressible Laminar Heat Transfer with Pressure Gradient. NACA TN 3888, 1956.

15. Van Driest, E. R.: Turbulent Boundary Layer in Compressible Fluids. Jour. Aero. Sci., vol. 18, no. 3, Mar. 1951, pp. 145-161.

16. Rubesin, Morris W.: A Modified Reynolds Analogy for the Compressible Turbulent Boundary Layer on a Flat Plate. NACA TN 2917, 1953.

17. Lees, L.: Laminar Heat Transfer Over Blunt-Nosed Bodies at Hypersonic Flight Speeds. Jet Prop., vol. 26, no. 4, Apr. 1956, pp. 259-269; 274.

18. Romig, Mary F.: Stagnation Point Heat Transfer for Hypersonic Flow. Jet Prop., vol. 26, no. 12, Dec. 1956, pp. 1098-1101.

19. Van Driest, E. R.: On Skin Friction and Heat Transfer Near the Stagnation Point. Rep. No. AL-2267, North Am. Aviation, Inc., Mar. 1956.

20. Dunn, D. W., and Lin, C. C.: On the Stability of the Laminar Boundary Layer in a Compressible Fluid. Jour. Aero. Sci., vol. 22, no. 7, July 1955, pp. 455-477.

21. Moorman, Emily P.: Free-Flight Rocket Material Characteristics. Rep. No. A-10-a, Res. and Dev. Div., Ord. Missile Labs., Redstone Arsenal, Huntsville (Ala.). (Revised June 1, 1956.)

TABLE I. - TWO-STAGE TEST BODIES - PHYSICAL DATA

	Model		
	A	B	C
Gross weight at launching (both stages less igniters), lb	469.0	451.35	456.48
Gross weight of second stage (less igniters), lb	76.2	76.05	80.3
Gross weight of booster (with coupling assembly, less igniters), lb	392.8	357.3	376.18
Coupling assembly weight, lb	1.95	4.8	5.2
Weight of second stage at burnout, lb	42.4	42.05	45.3
Telemeter package weight, lb	16.3	16.1	18.7
Center of gravity at launching[a], in.	106.6	101.8	104.5
Center of gravity at first-stage burnout[a], in.	92.5	87.3	90.0
Center of gravity of second-stage after separation[a], in.	37.5	34.0	34.80
Center of gravity of second-stage after burnout[a], in.	33.4	29.7	29.9
Booster fin area (2 fins), sq in.	262	287.9	287.9
Second-stage flare angle, semicone, deg	10	10	10
Body diameter, booster, in.	9.00	9.00	9.00
Body diameter, second stage, in.	6.00	6.00	6.00
Tip diameter, nose cone, in.	2	3	4
Included cone angle, second stage, deg	15	15	15
Skin material, second stage:			
Cone	Nickel	Inconel	Inconel
Cylinder	Inconel	Inconel	Inconel
Hemispheric tip	Nickel	Nickel	Nickel
Surface finish of instrumented cone cylinder, average roughness height, microin.			
Cone	2	2	2
Cylinder	2	2	2
Hemispheric tip	2	2	2

[a]From nose tip.

TABLE II. - ROCKETS

[Ref. 21.]

Rocket	Gross weight, lb	Propellant weight, lb	Average thrust, lb	Impulse, lb-sec	Gross weight specific impulse, sec	Propellant specific impulse, sec	Burning time, sec
Sustainer (T-55)	45.8	33.5	[a]3,900	[a]6,950	[a]152	[a]208	[a]1.60
Booster (T-64)	377.2	270.0	[b]33,900	[b]51,600	[b]145	[b]218	[b]1.52

[a]At -20° F and sea level.
[b]At 70° F.

TABLE III. - TRANSITION SUMMARY

(a) Model B

Station	1	2	3	4	5	6	7	8	9	[a]10
Location	Stagnation	$\theta = 45^\circ$	Cone	Cone	Cone	Cone	Cyl.	Cyl.	Cyl.	Cone
Type of transition	----------	--------	[b]L/T	L/T	L/T	L/T	L/T	L/T	L/T	L/T
Transition time, sec	----------	--------	1.10	1.10	1.10	1.10	0.90	0.90	0.90	0.75
t_w/t_l	----------	--------	0.58	0.58	0.58	0.58	0.825	0.81	0.796	0.813
Re_l	----------	--------	0.77×10^6	1.58×10^6	2.38×10^6	3.19×10^6	3.17×10^6	4.34×10^6	5.57×10^6	3.39×10^6
M_l	----------	--------	2.30	2.30	2.30	2.30	2.46	2.42	2.40	1.95

(b) Model C

Station	1	2	3	4	5	6	7	8	[a]9	[a]10
Location	$\theta = 22\frac{1}{2}^\circ$	$\theta = 45^\circ$	Cone	Cone	Cone	Cyl.	Cyl.	Cyl.	Cone	Cyl.
Type of transition	----------	L/T	L/T	L/T	L/T	L/T	L/T	L/T	L/T	L/T
Transition time, sec	----------	1.35	1.00	1.00	1.00	1.00	1.00	1.00	1.00	1.00
t_w/t_l	----------	0.27	0.67	0.67	0.68	0.82	0.78	0.78	0.67	0.77
Re_l	----------	0.60×10^6	0.996×10^6	1.66×10^6	2.32×10^6	2.20×10^6	3.42×10^6	4.94×10^6	2.32×10^6	4.94×10^6
M_l	----------	1.05	2.20	2.20	2.20	2.59	2.47	2.48	2.20	2.48
Type of transition	----------	[c]T/L	T/L	T/L	T/L	--------	--------	T/L	T/L	T/L
Transition time, sec	----------	[d]2.20	5.00	5.20	5.40	--------	--------	5.60	5.50	6.60
t_w/t_l	----------	0.27	0.79	0.82	0.89	--------	--------	1.10	0.83	1.30
Re_l	----------	0.71×10^6	1.01×10^6	1.72×10^6	2.49×10^6	--------	--------	3.24×10^6	2.54×10^6	4.99×10^6
M_l	----------	1.08	2.84	2.82	2.84	--------	--------	3.38	2.80	3.10
Type of transition	----------	--------	--------	--------	L/T	--------	--------	L/T	--------	--------
Transition time, sec	----------	--------	--------	--------	6.90	--------	--------	6.80	--------	--------
t_w/t_l	----------	--------	--------	--------	1.48	--------	--------	1.51	--------	--------
Re_l	----------	--------	--------	--------	3.20×10^6	--------	--------	5.18×10^6	--------	--------
M_l	----------	--------	--------	--------	2.57	--------	--------	3.01	--------	--------

[a]Stations 180° from mainline of instrumentation.
[b]L/T Laminar to turbulent.
[c]T/L Turbulent to laminar.
[d]Estimated time of possible transition.

Station	Station, in.	Wetted surface distance, in.	Skin material[a]	Skin thickness, in.	α, deg
1	0.06	0.349	Nickel	0.125 Plug in solid tip	290
2	4.00	4.598		0.0525	270
3	6.86	7.48		.0505	270
4	9.734	10.382		.0540	270
5	12.601	13.274		.0552	270
6	15.556	16.255		.0502	270
7	17.843	18.548	Inconel	.0272	270
8	22.899	23.604		.0290	270
9	27.955	28.660		.0312	270
10	15.556	16.255		.0610	90

[a]Surface finish: 2 microin. average surface roughness.

Instrumentation	
Quantity	Range
Skin temperature	400° to 1600° R, 400° to 2400° R
Cone pressure	2 to 15 lb/sq in. abs
Stagnation pressure (total)	2 to 350 lb/sq in. abs
Axial acceleration	0 to +160 g's
Axial acceleration	+1 to -40 g's

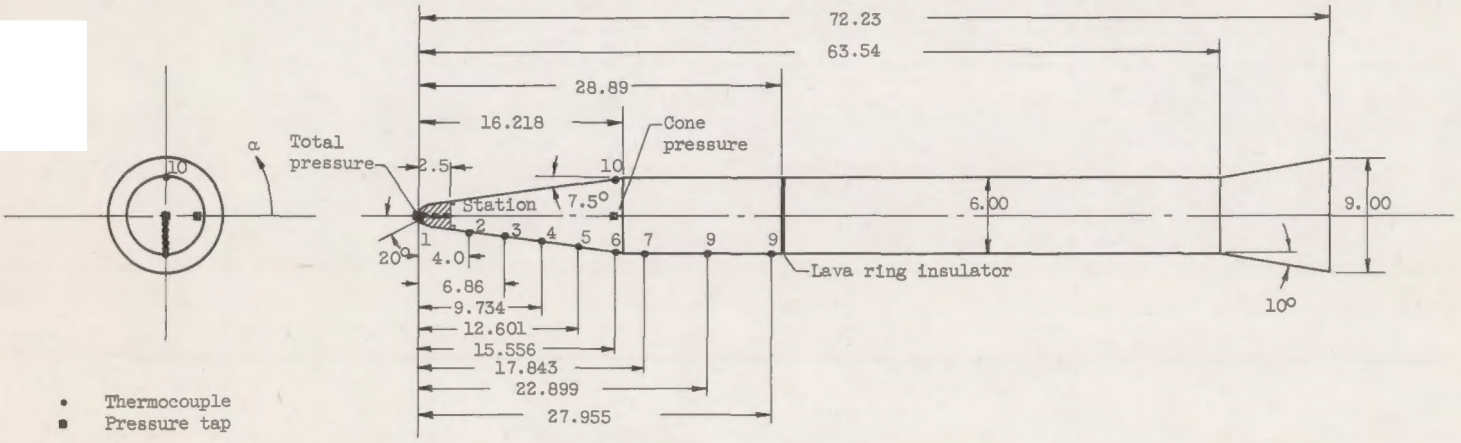

(a) Model A, 2-inch-diameter tip.

Figure 1. - Sketch of test body showing instrumentation locations and skin thicknesses at each station. (All dimensions are in inches.)

Station	Station, in.	Wetted surface distance, in.	Skin material[a]	Skin thickness, in.	α, deg
1	0	0	Nickel	0.125 Plug in solid tip	0
2	.44	1.178	Nickel	0.125 Plug in solid tip	157.5
3	2.31	3.175	Inconel	0.0700	270
4	5.607	6.500		.0675	270
5	8.904	9.826		.0645	270
6	12.201	13.151		.0635	270
7	14.201	15.156		.0305	270
8	19.351	20.306		.0295	270
9	24.501	25.457		.0310	270
10	12.201	13.151		.0630	90

[a]Surface finish: 2 microin. average surface roughness.

Instrumentation	
Quantity	Range
Skin temperature	400° to 1600° R; 400° to 2400° R
Cone pressure	1 to 15 lb/sq in. abs
Cylinder pressure	1 to 15 lb/sq in. abs
Axial acceleration	0 to +160 g's
Axial acceleration	+1 to -40 g's

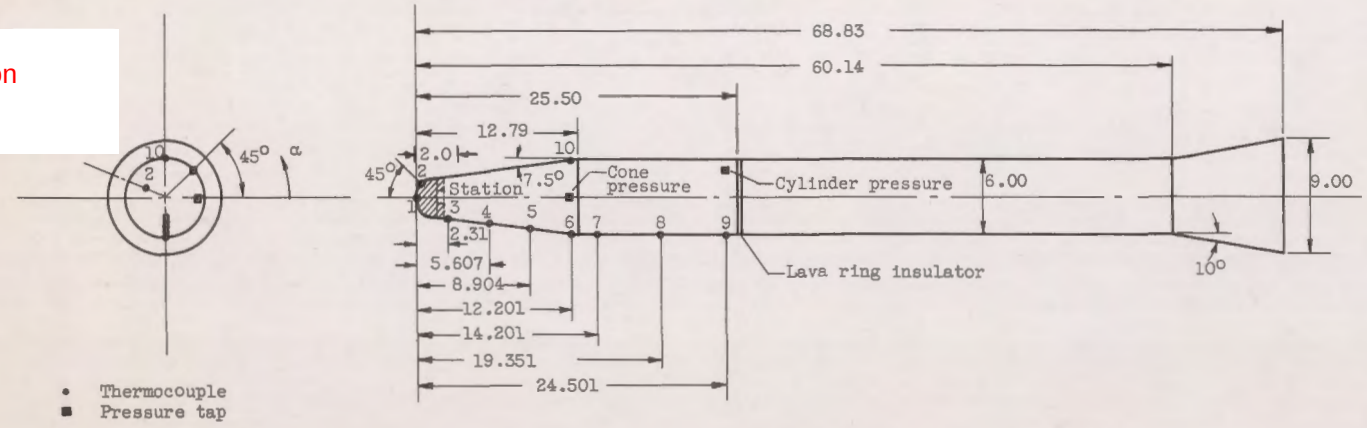

(b) Model B, 3-inch-diameter tip.

Figure 1. - Continued. Sketch of test body showing instrumentation locations and skin thicknesses at each station. (All dimensions are in inches.)

Station	Station, in.	Wetted surface distance, in.	Skin material[a]	Skin thickness, in.	α, deg
1	0.152	0.785	Nickel	0.375	270
2	.536	1.570	↓	.375	270
3	3.125	4.279	Inconel	.067	270
4	5.937	7.115	↓	.066	270
5	8.749	9.951	↓	.063	270
6	10.750	11.959	↓	.032	270
7	17.685	18.894	↓	.031	270
8	24.622	25.831	↓	.029	270
9	8.749	9.951	↓	.069	90
10	24.622	25.831	↓	.034	90

[a]Surface finish: 2 microin. average surface roughness.

Instrumentation	
Quantity	Range
Skin temperature	400° to 1600° R
Cone pressure	2 to 15 lb/sq in. abs
Stagnation pressure (total)	3 to 350 lb/sq in. abs
Axial acceleration	0 to +160 g's
Axial acceleration	+1 to -40 g's
Lateral acceleration (yaw)	±14 g's
Lateral acceleration (pitch)	±10 g's

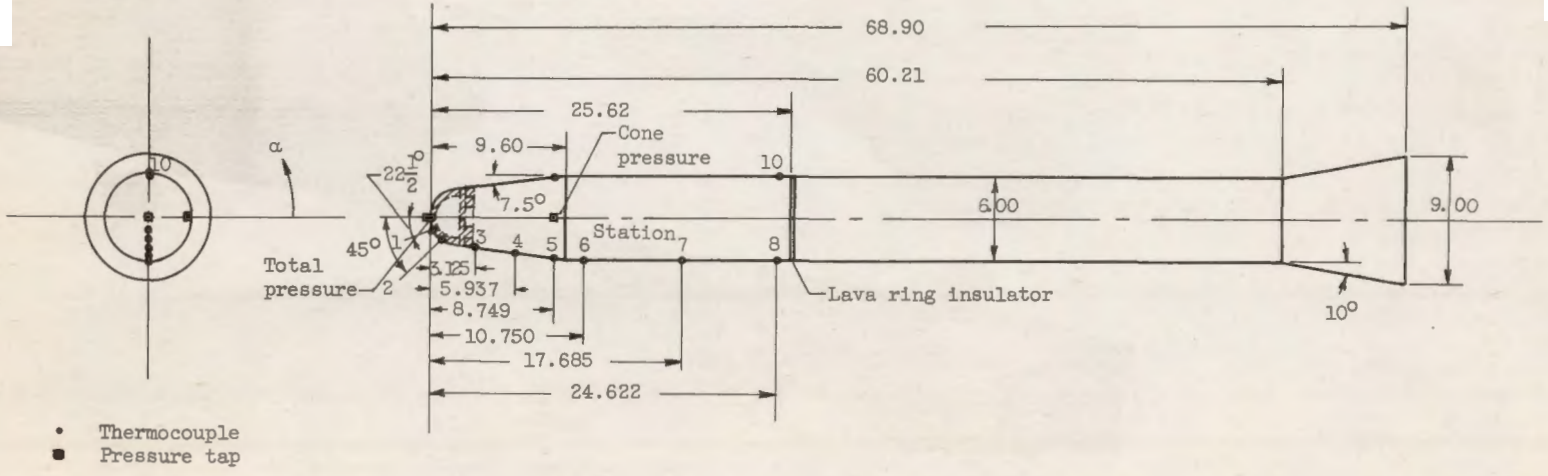

(c) Model C, 4-inch-diameter tip.

Figure 1. - Concluded. Sketch of test body showing instrumentation locations and skin thicknesses at each station. (All dimensions are in inches.)

Figure 2. - Typical test configuration and booster assembly (model A).

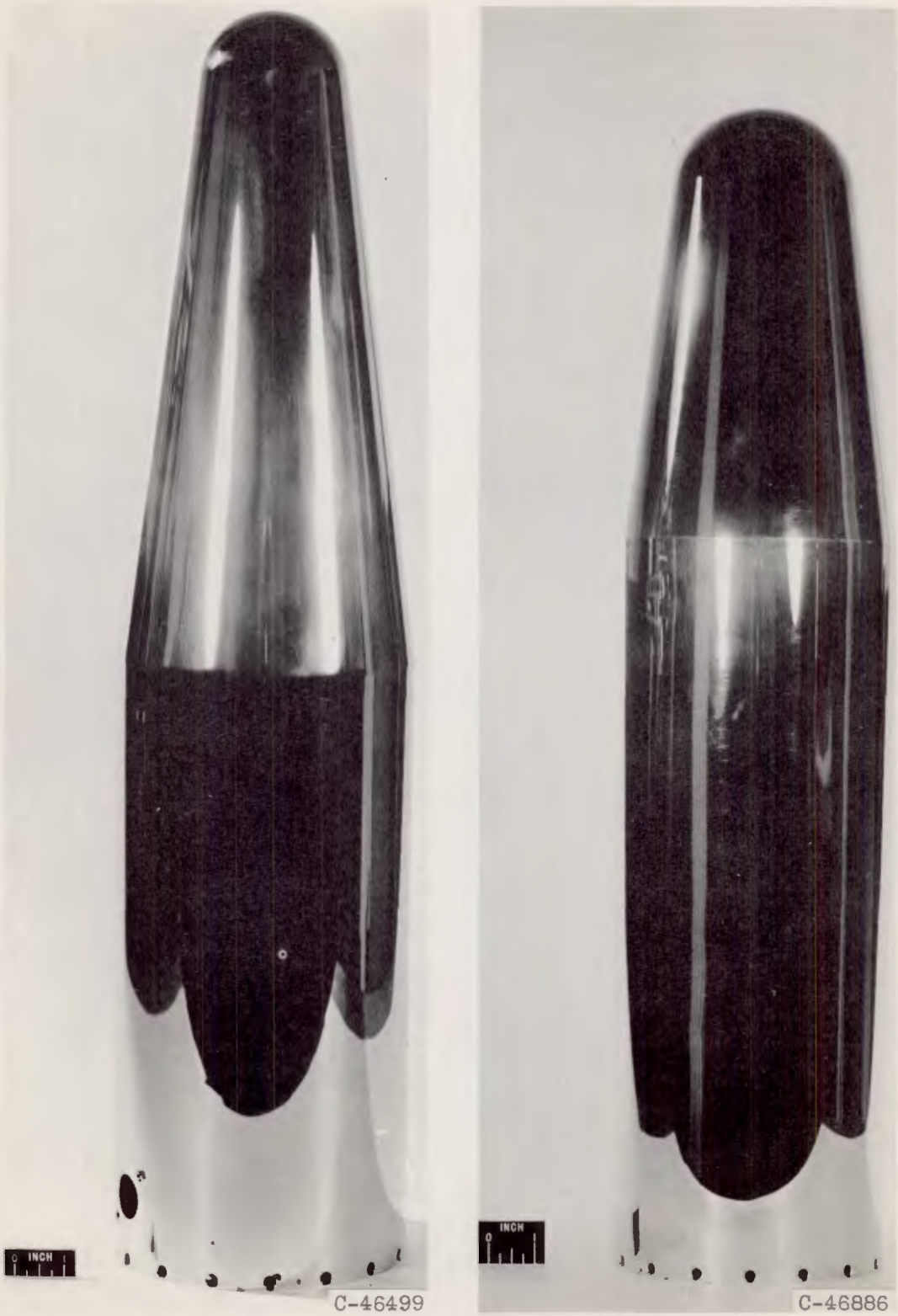

(a) Model B.

(b) Model C.

Figure 3. - Nose cone.

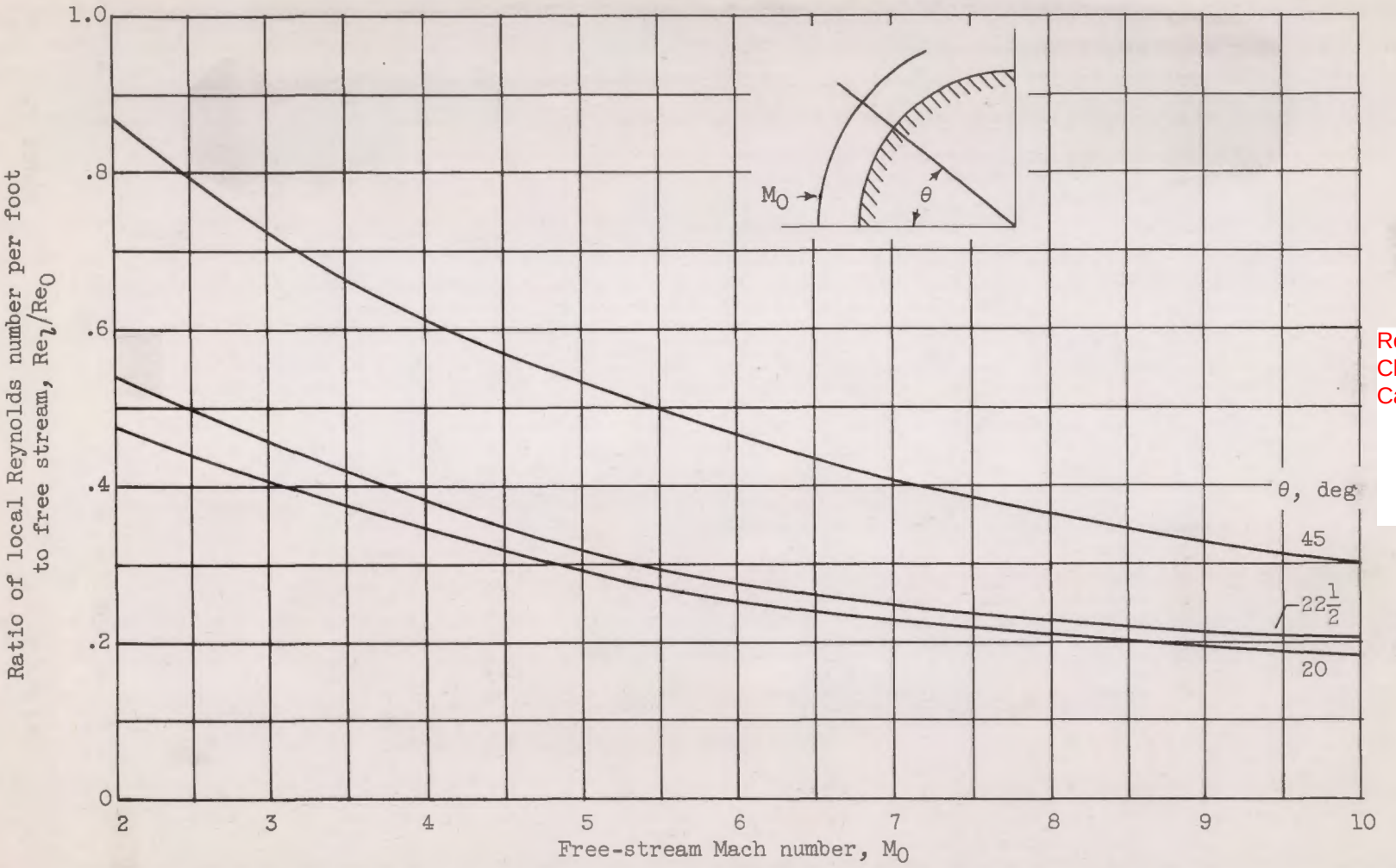

Figure 4. - Calculated Reynolds number variation along nose surface.

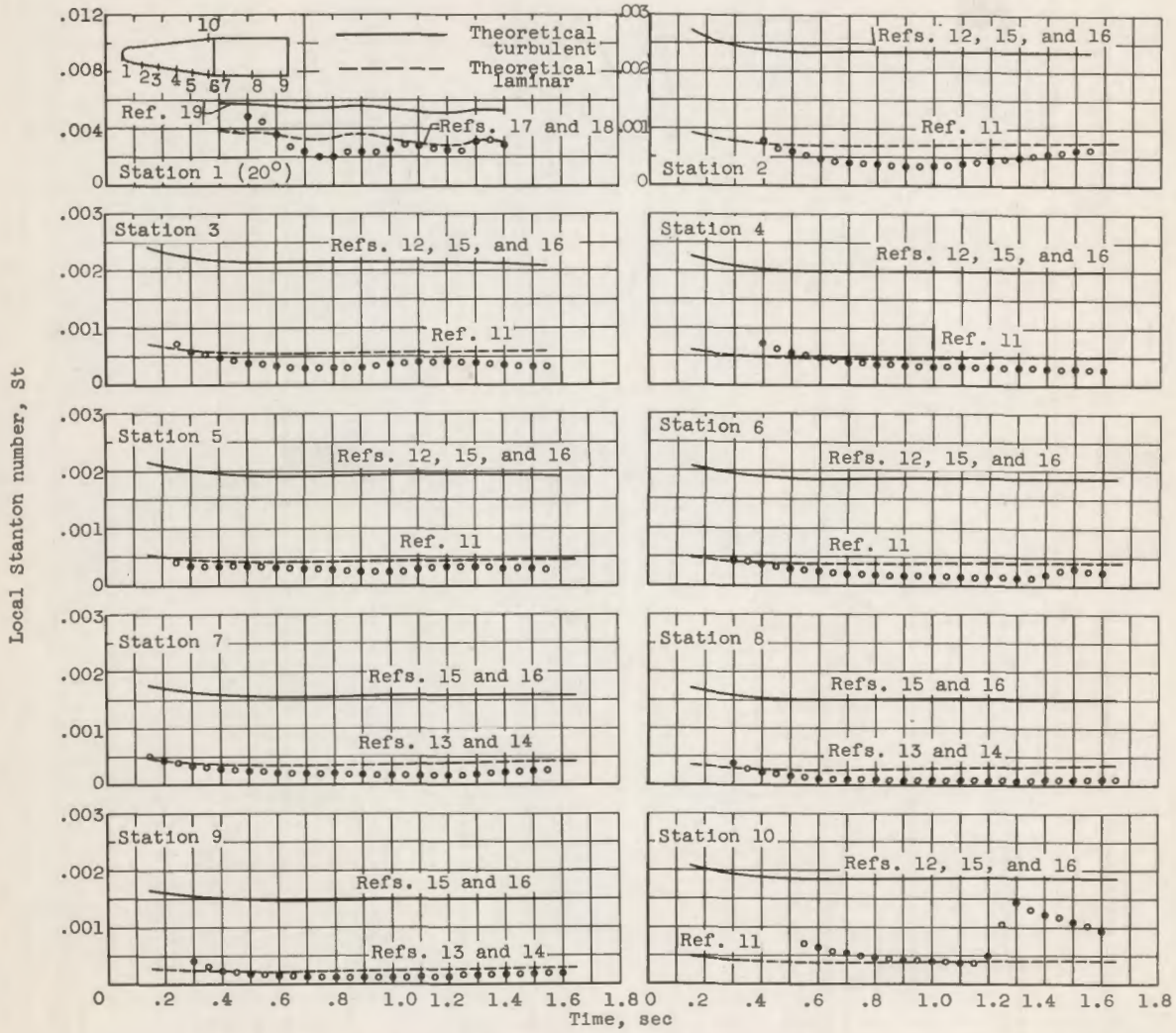

(a) Model A.

Figure 5. - Time history of local Stanton number.

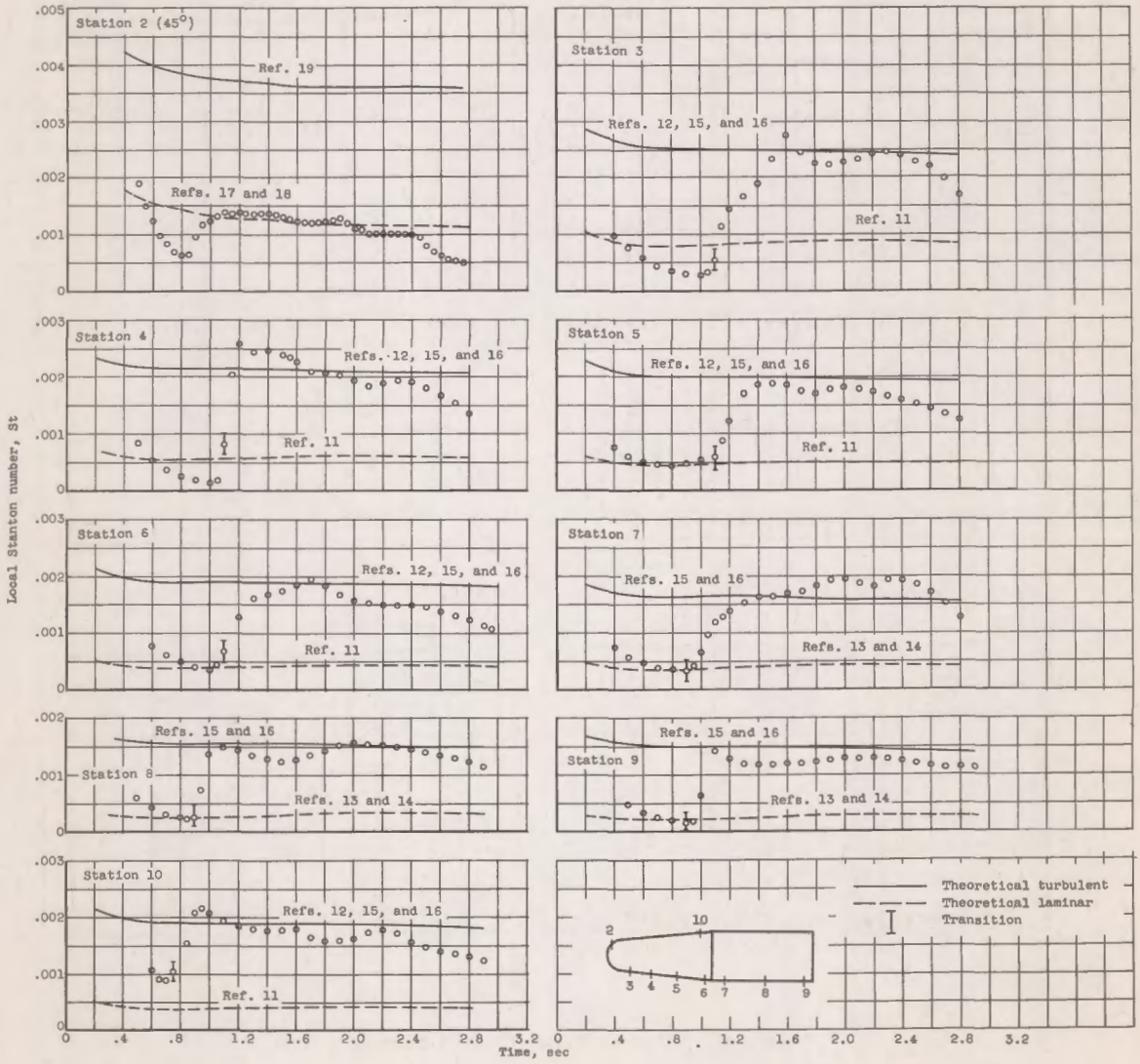

(b) Model B.

Figure 5. - Continued. Time history of local Stanton number.

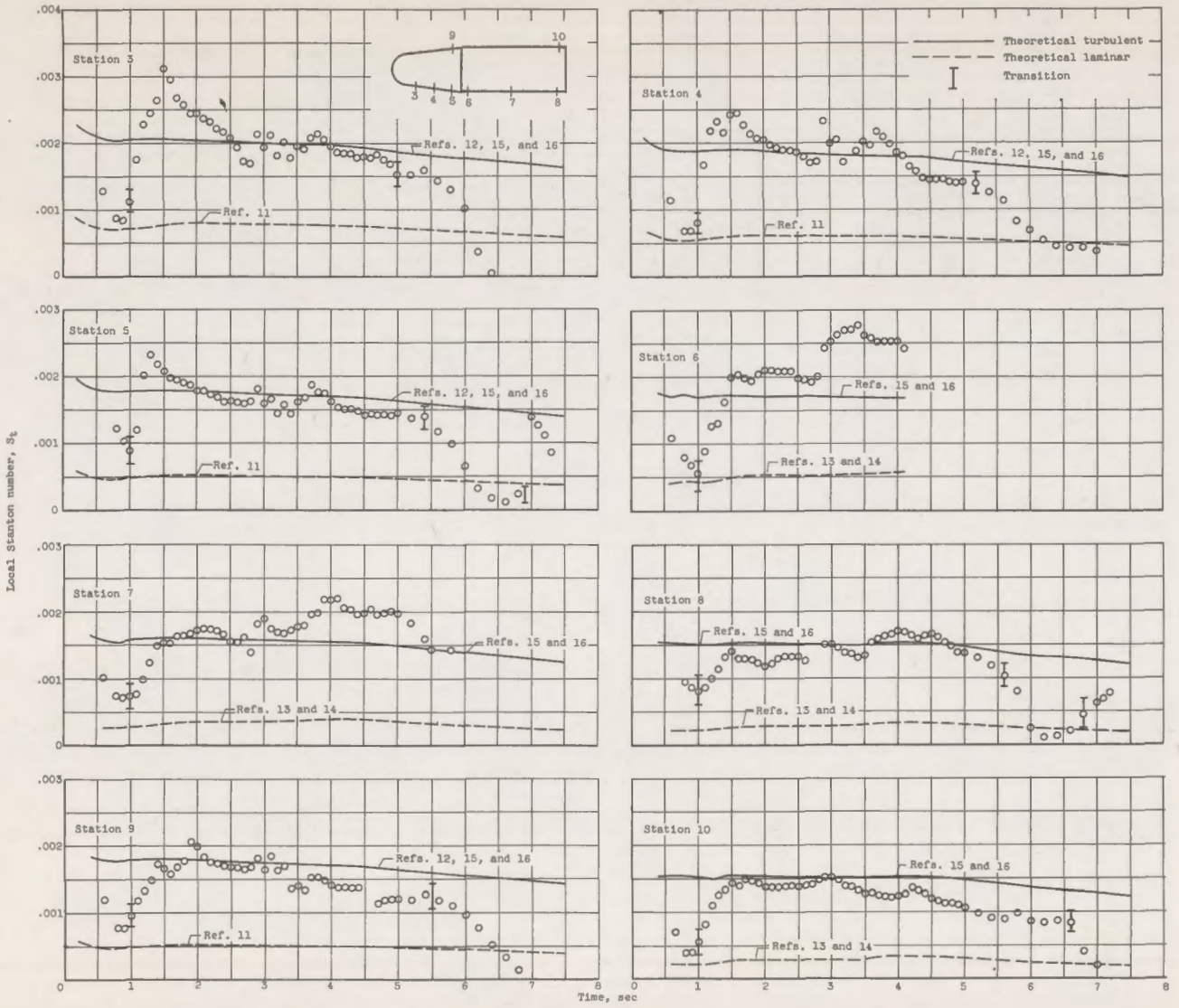

(c) Model C.

Figure 5. - Concluded. Time history of local Stanton number.

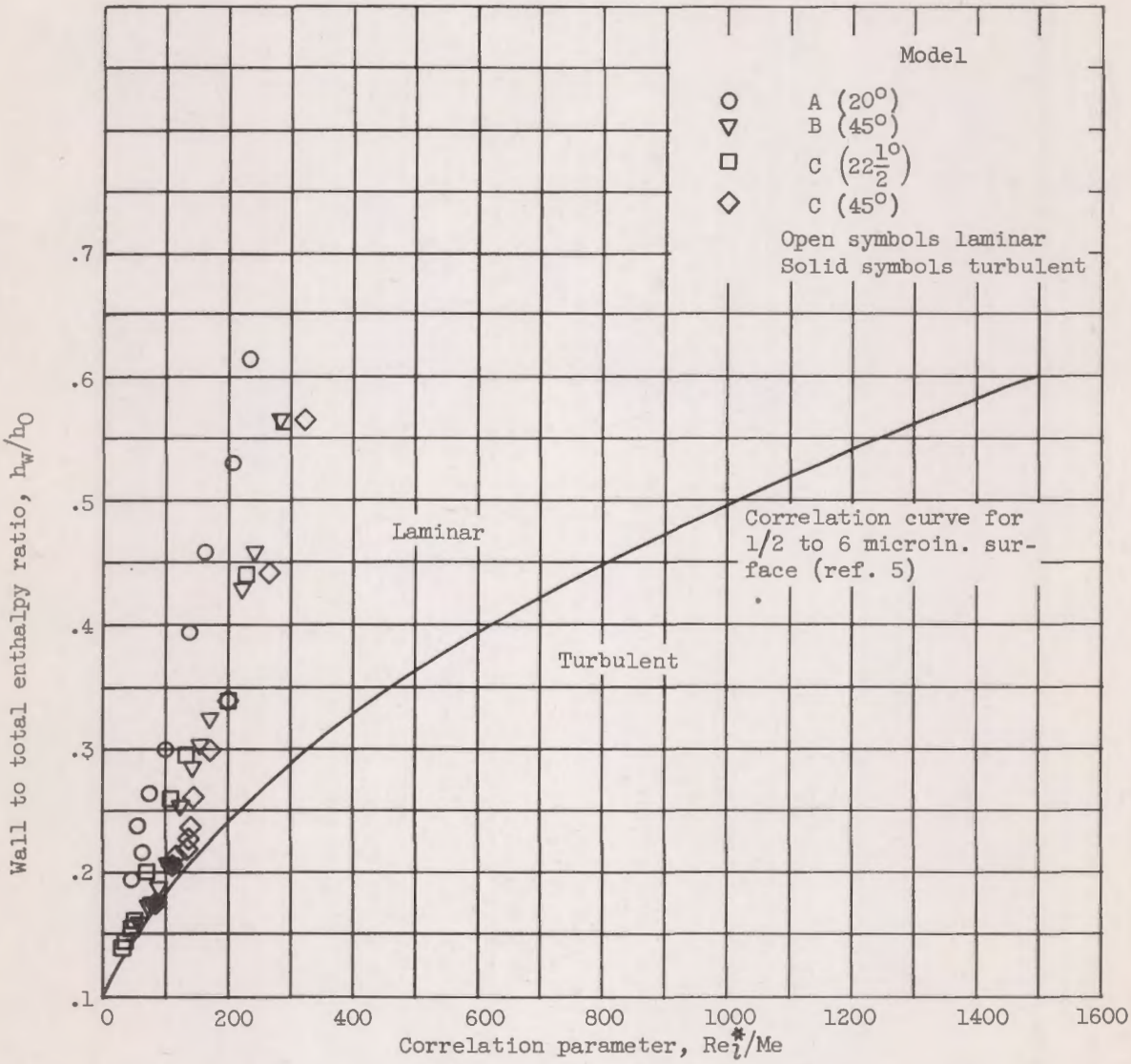

Figure 6. - Comparison of present flight data with correlation curve of reference 4.

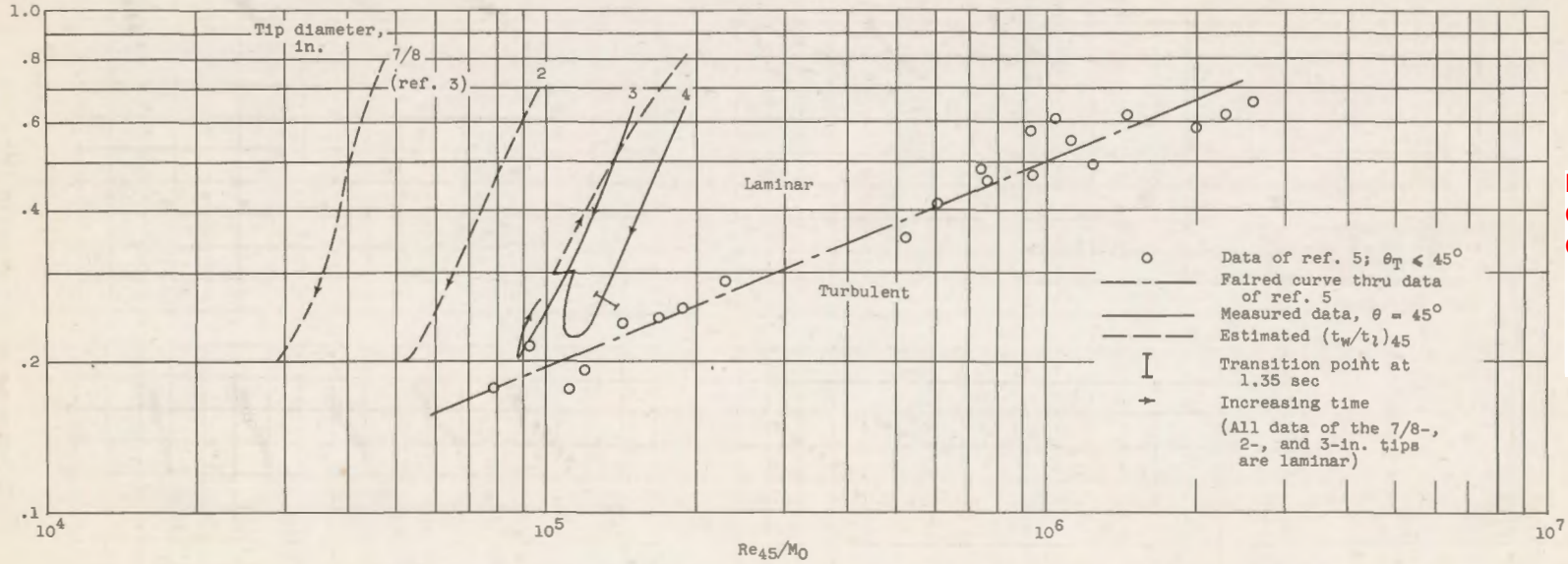

Figure 7. - Simplified correlation of some transition results on blunt noses.

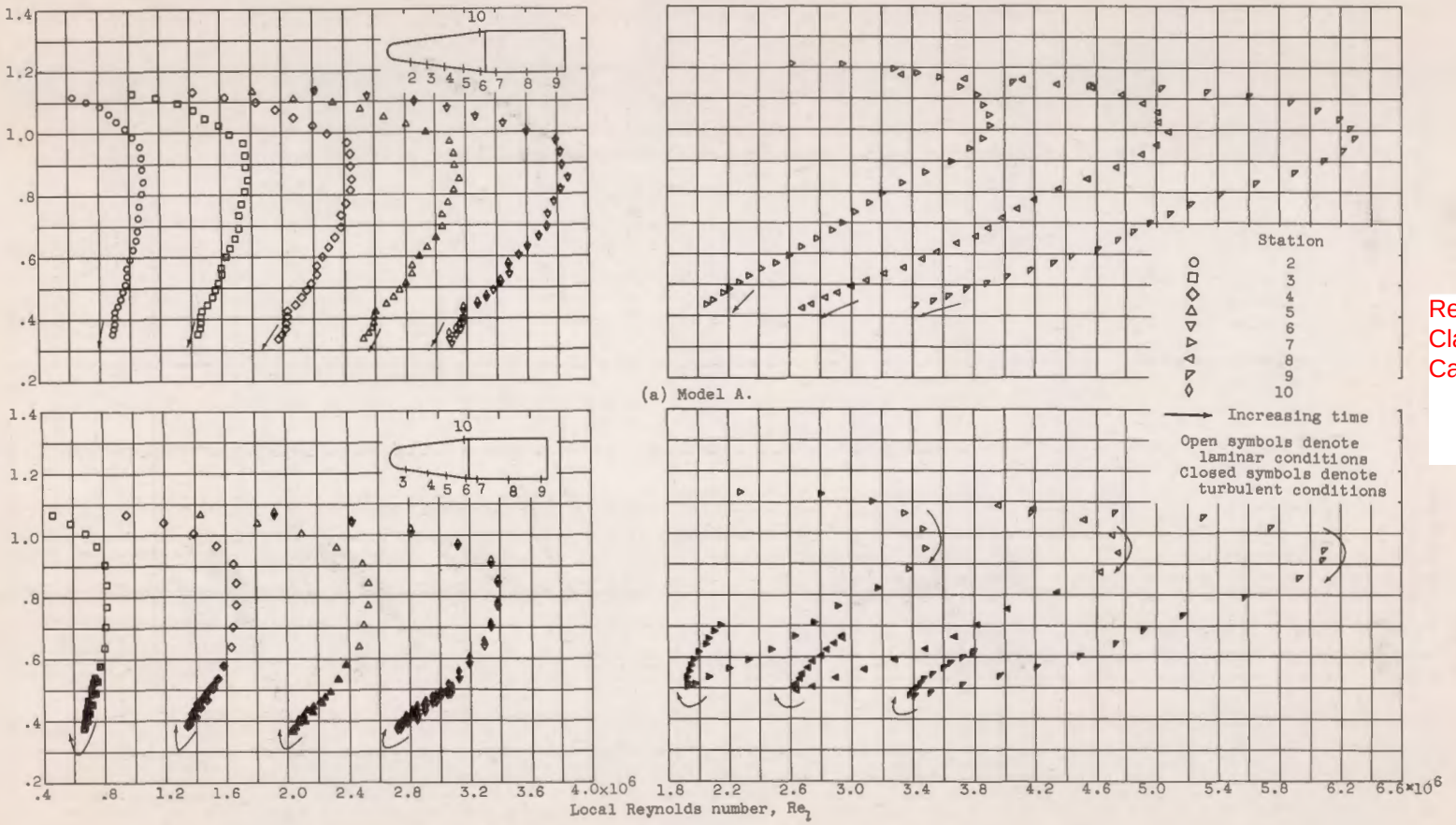

Figure 8. - Variation of local temperature ratio with local Reynolds number.

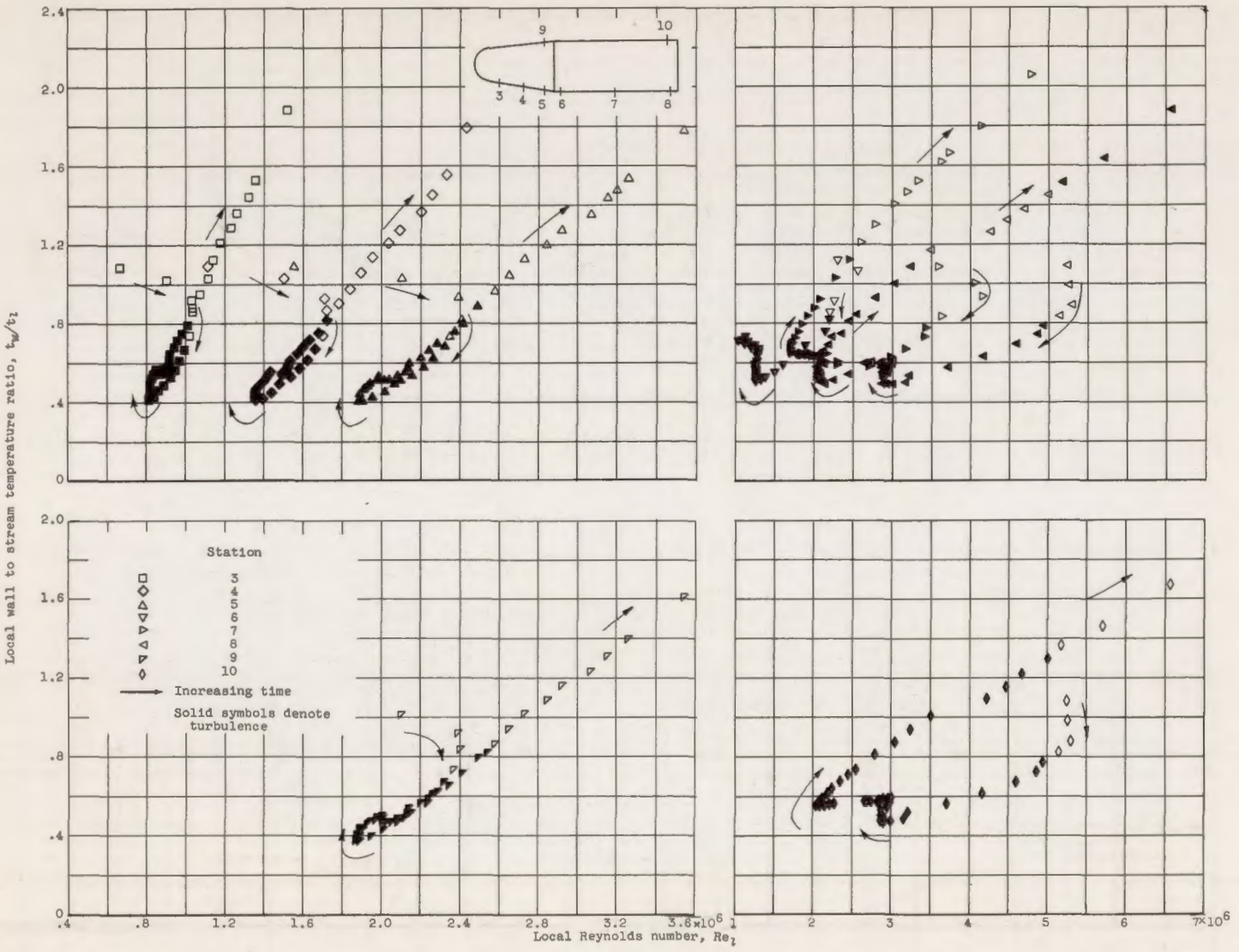

(c) Model C.

Figure 8. - Concluded. Variations of local temperature ratio with local Reynolds number.

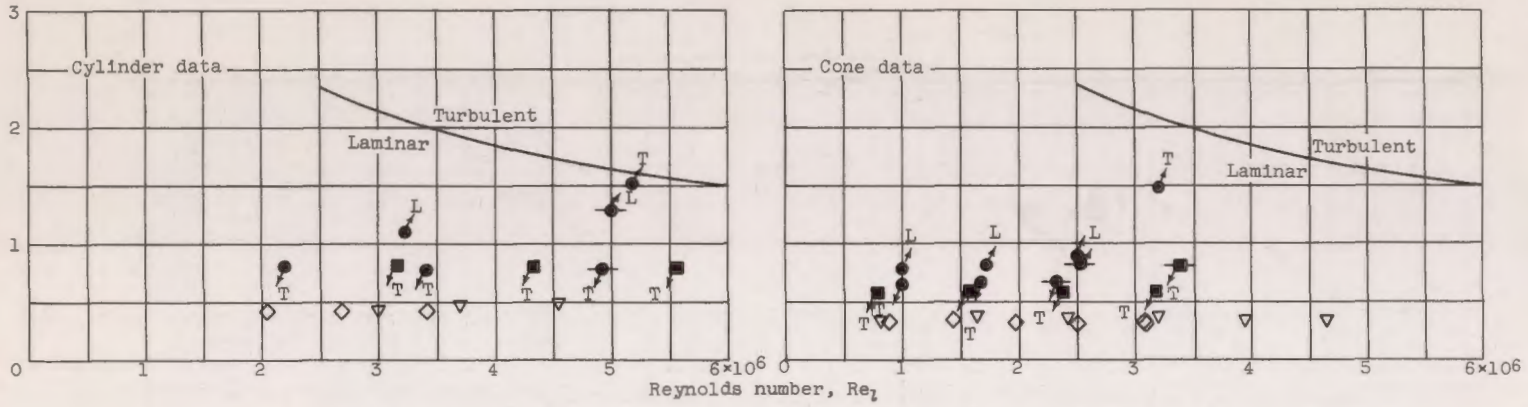

(a) Wall to local stream temperature ratio against Reynolds number.

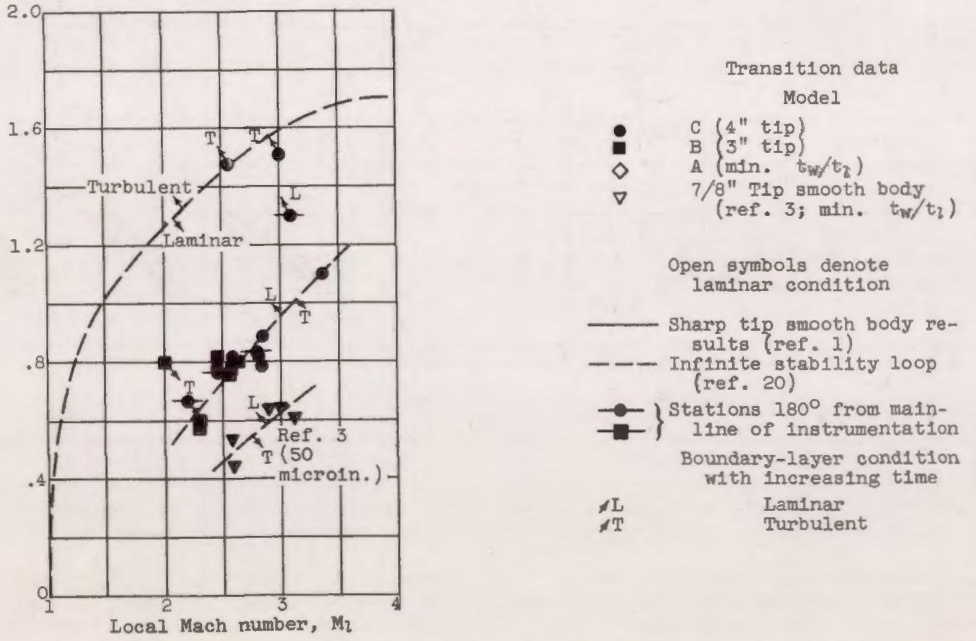

(b) Wall to local stream temperature ratio against local Mach number.

Figure 9. - Summary of transition data.

CON

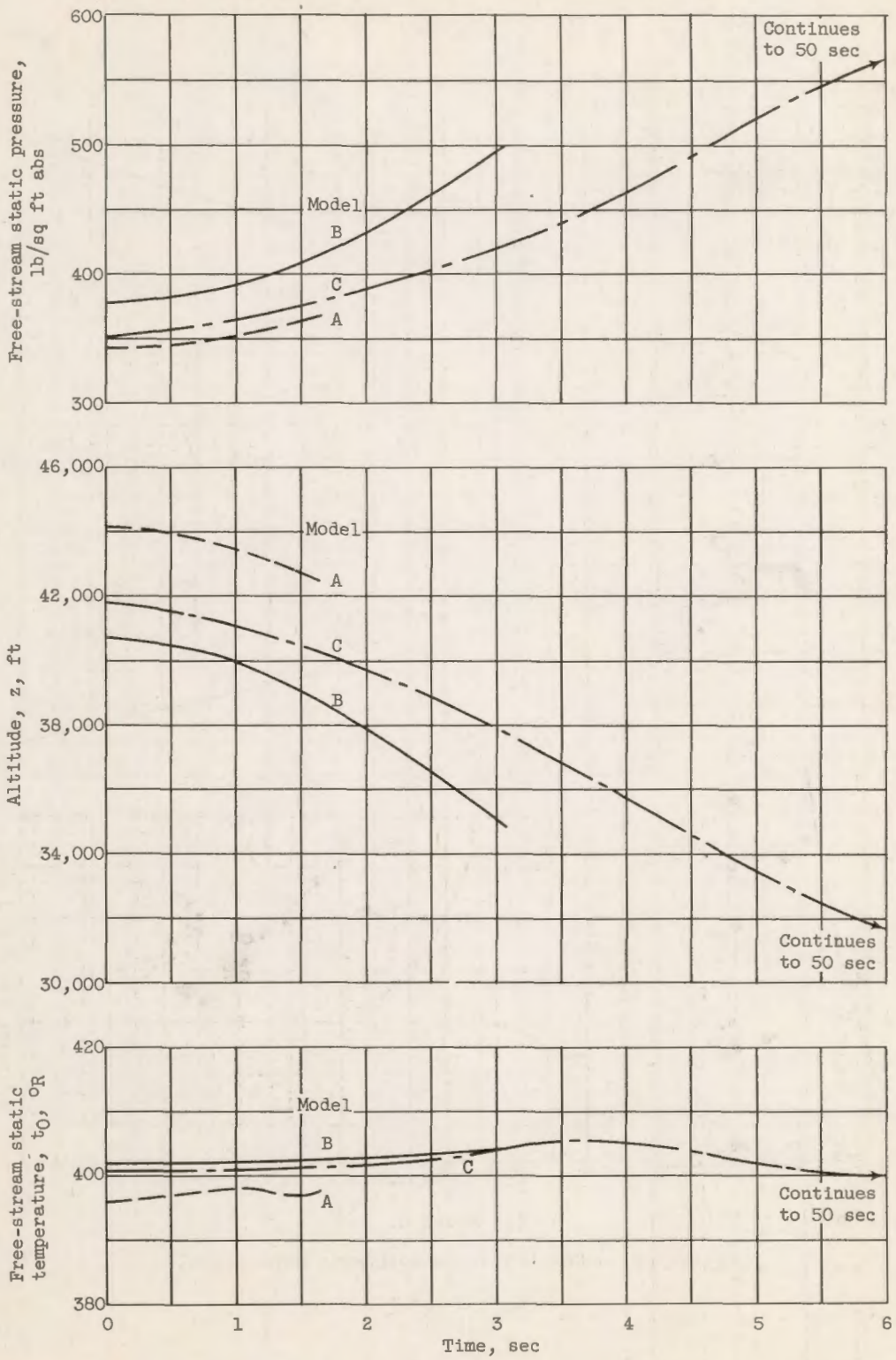

(a) Models A, B, and C.

Figure 10. - Atmospheric conditions.

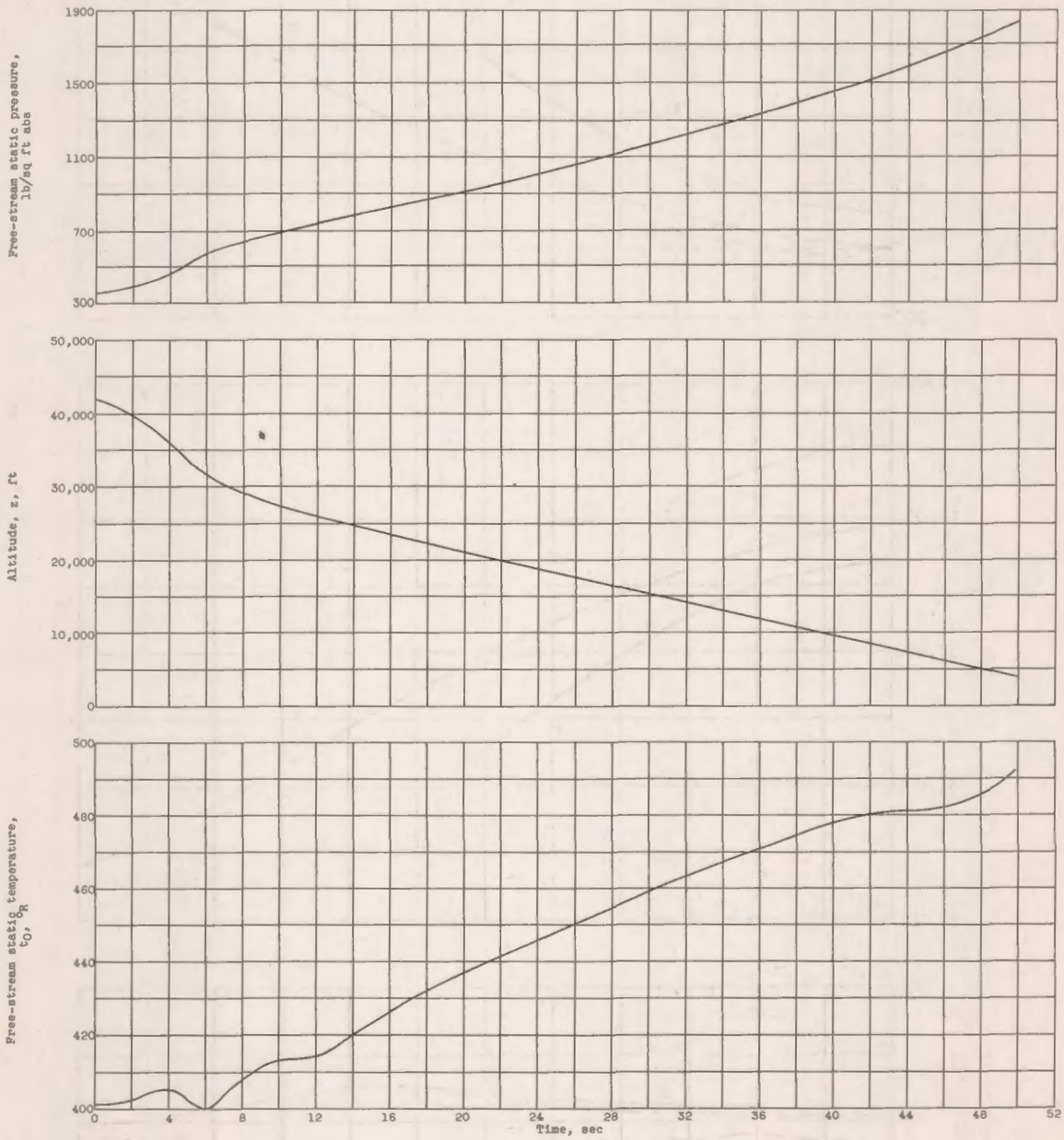

(b) Model C.

Figure 10. - Concluded. Atmospheric conditions.

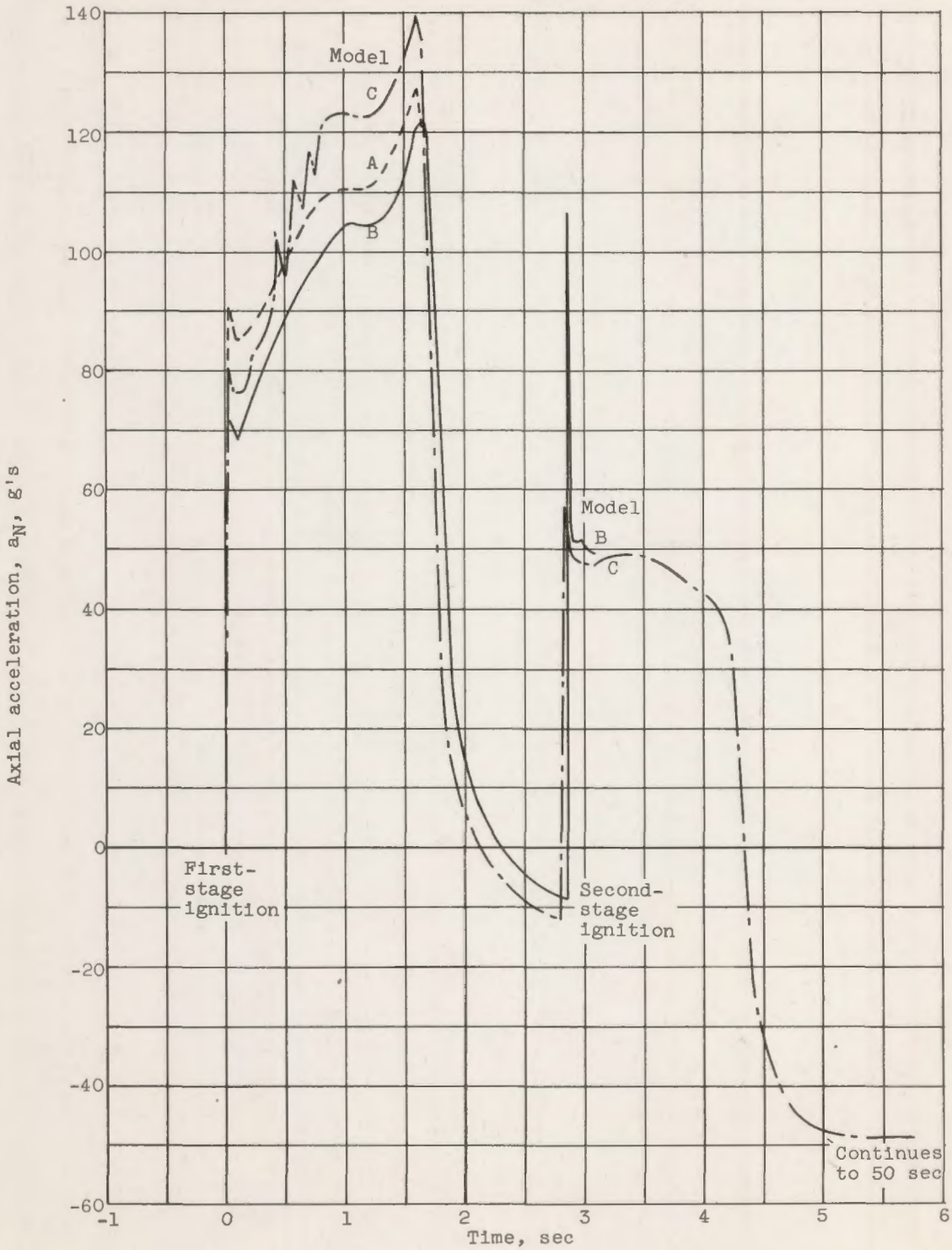

Figure 11. - Time history of axial and lateral acceleration.

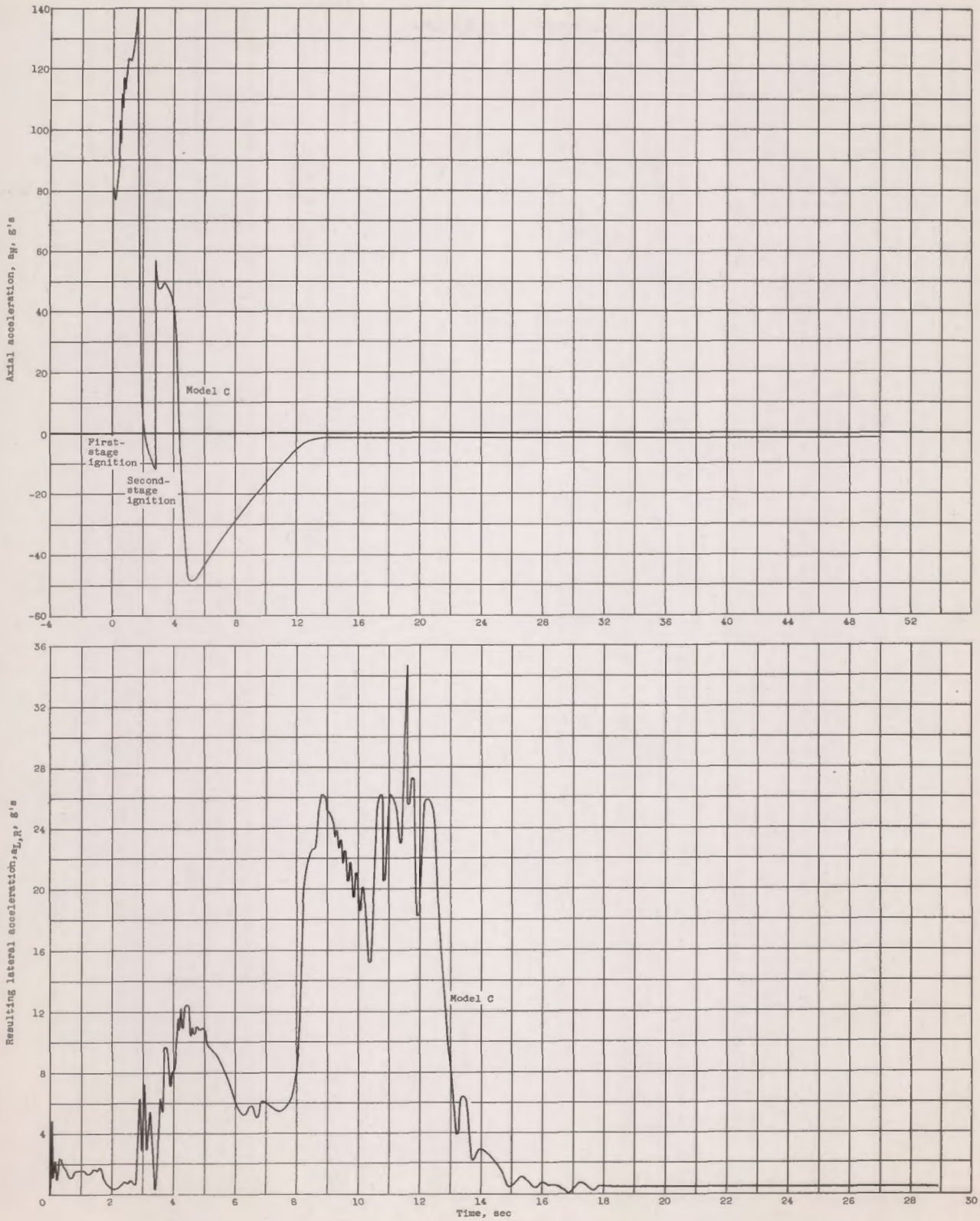

Figure 11. - Concluded. Time history of axial and lateral acceleration.

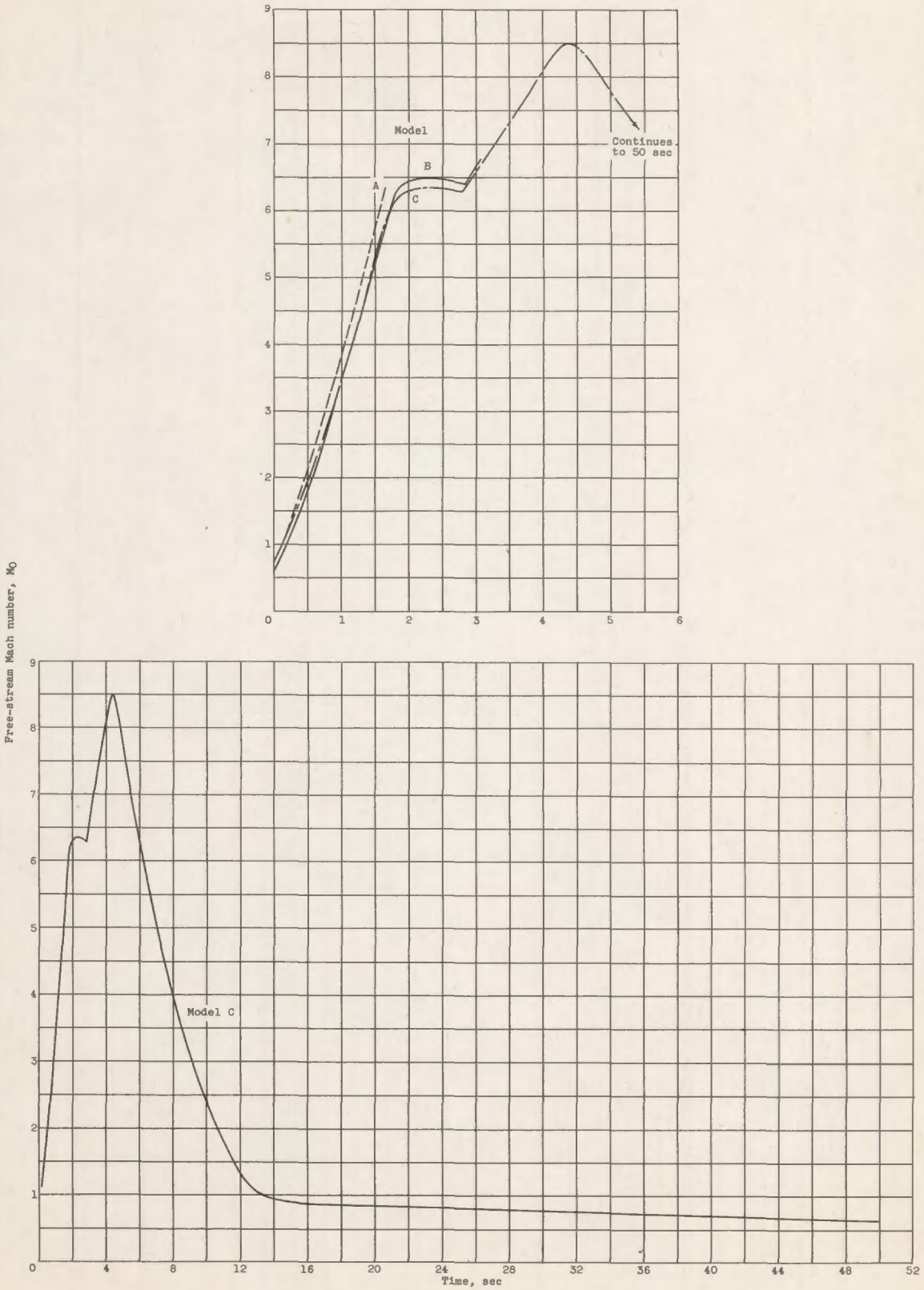

Figure 12. - Variation of free-stream Mach number with time.

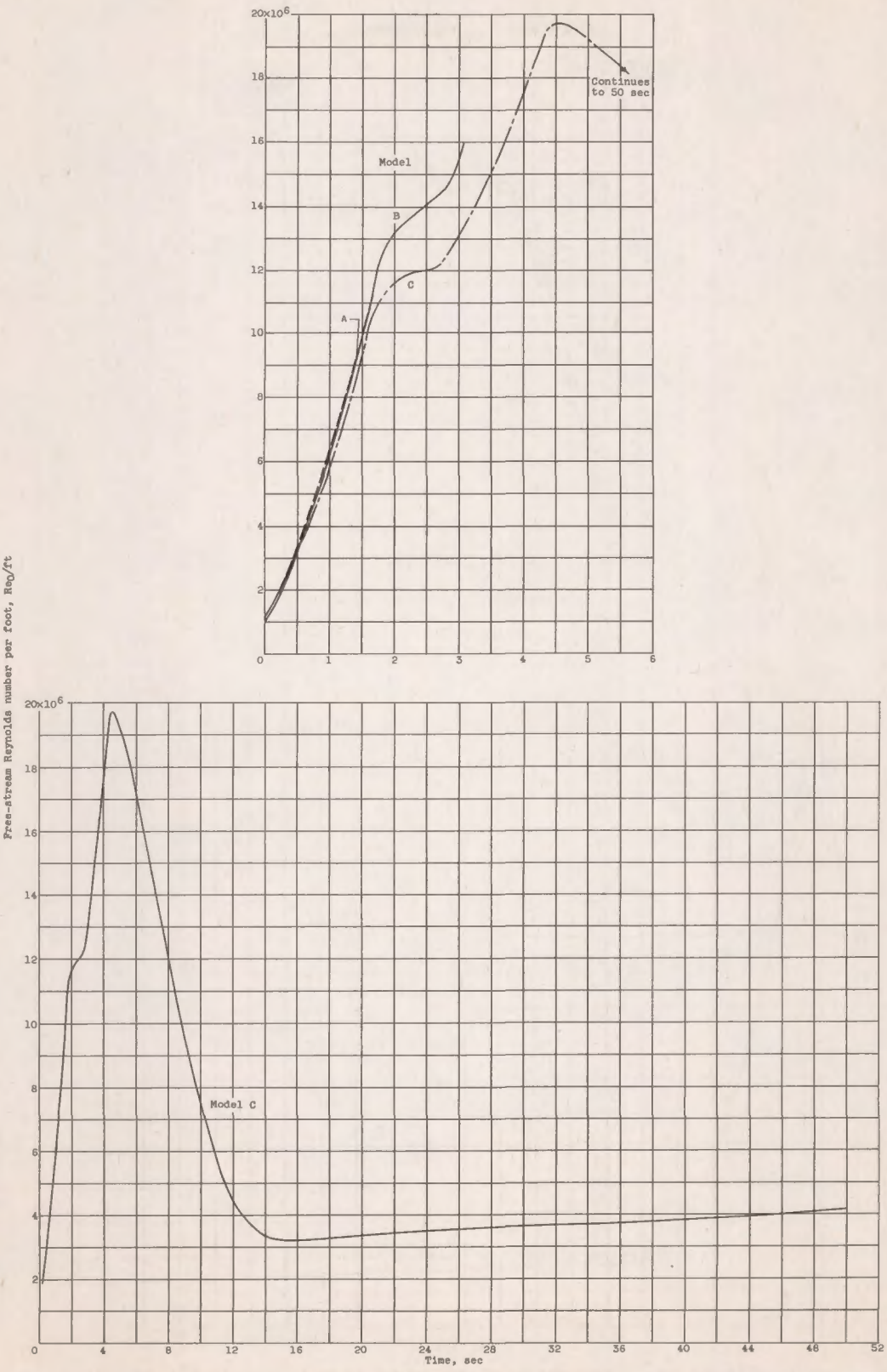

Figure 13. - Variation of free-stream Reynolds number per foot with time.

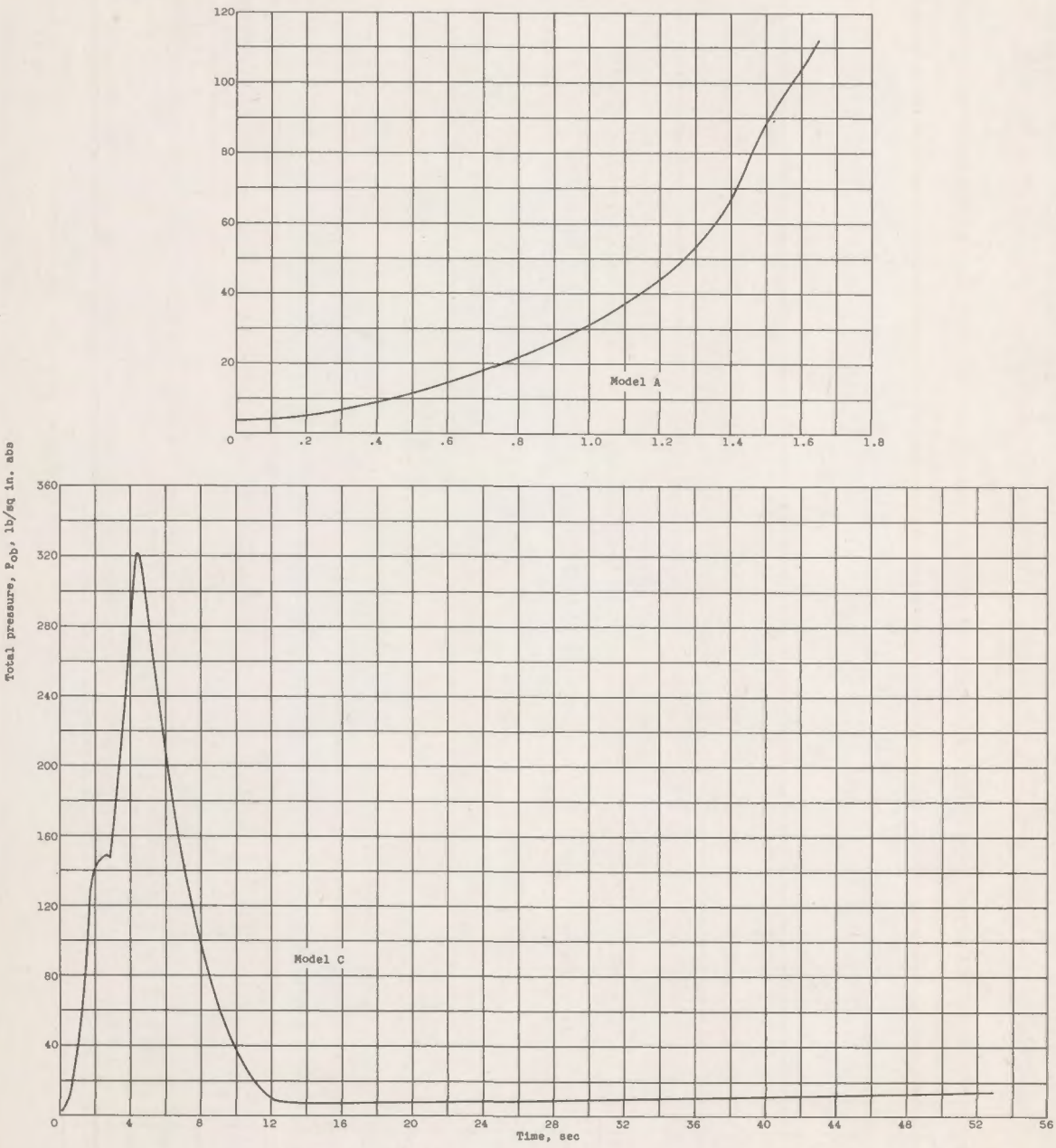

Figure 14. - Variation of free-stream total pressure with time.

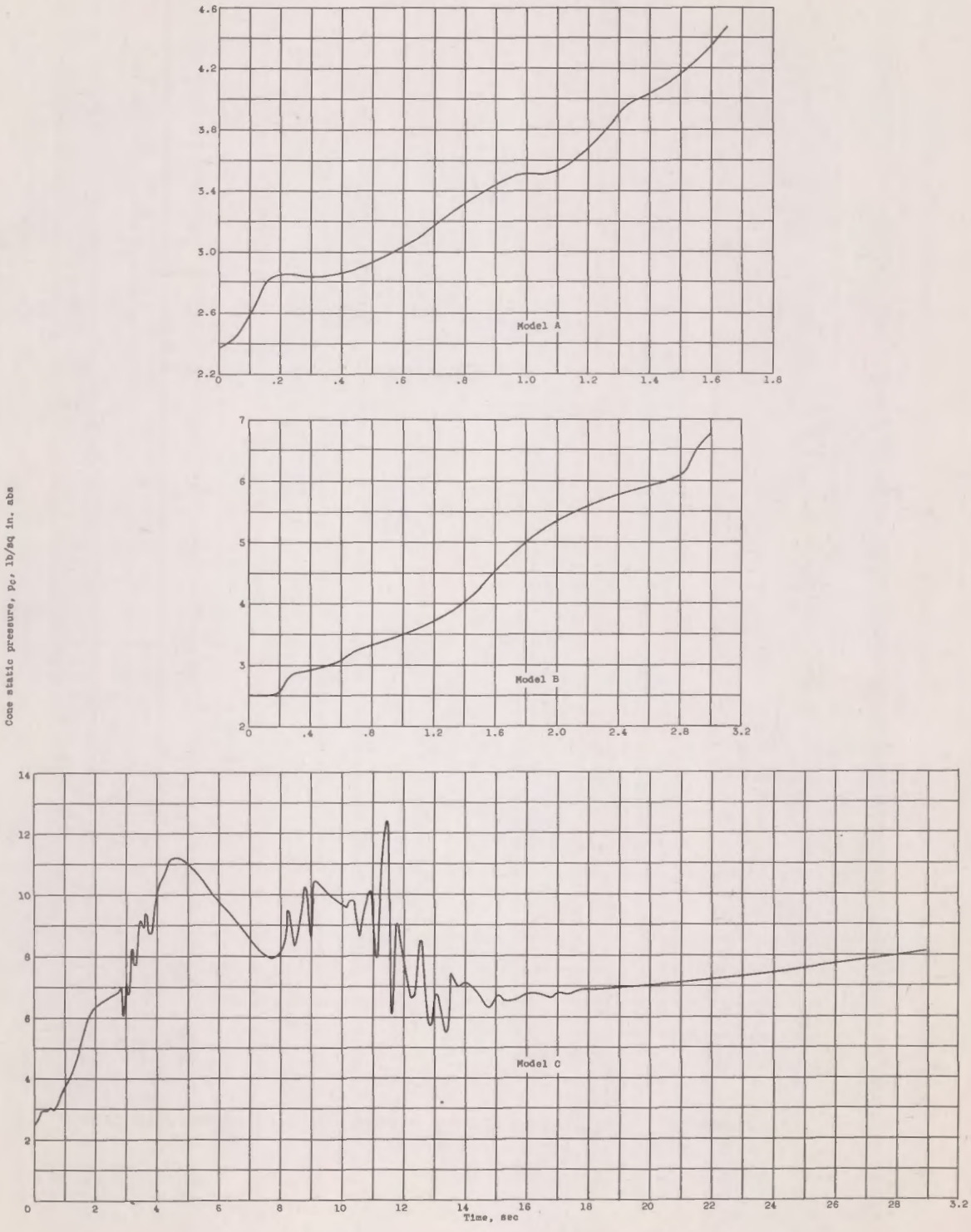

Figure 15. - Time history of cone static pressure for models A, B, and C.

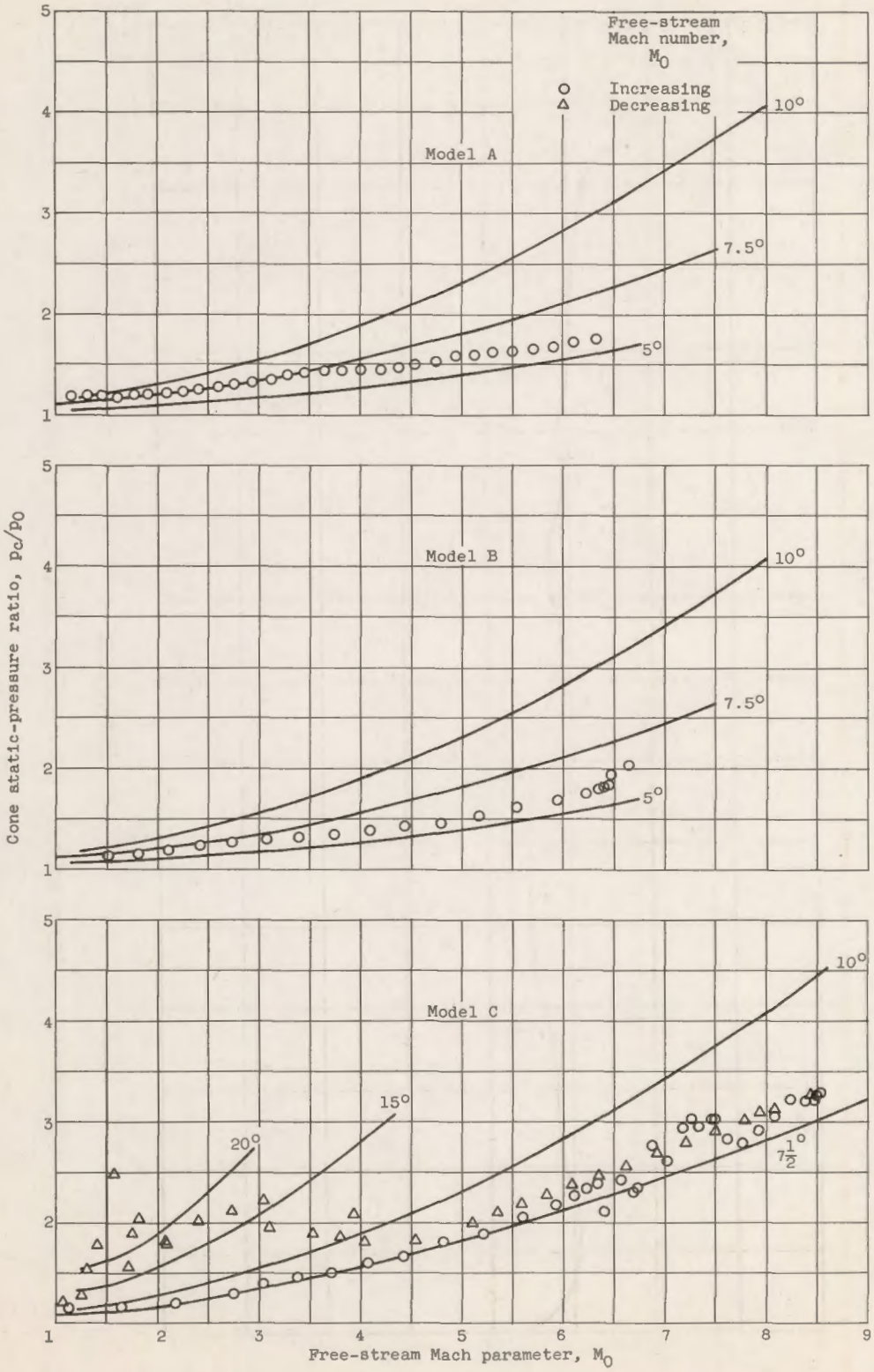

Figure 16. - Cone static-pressure ratio against free-stream Mach number, models A, B, and C.

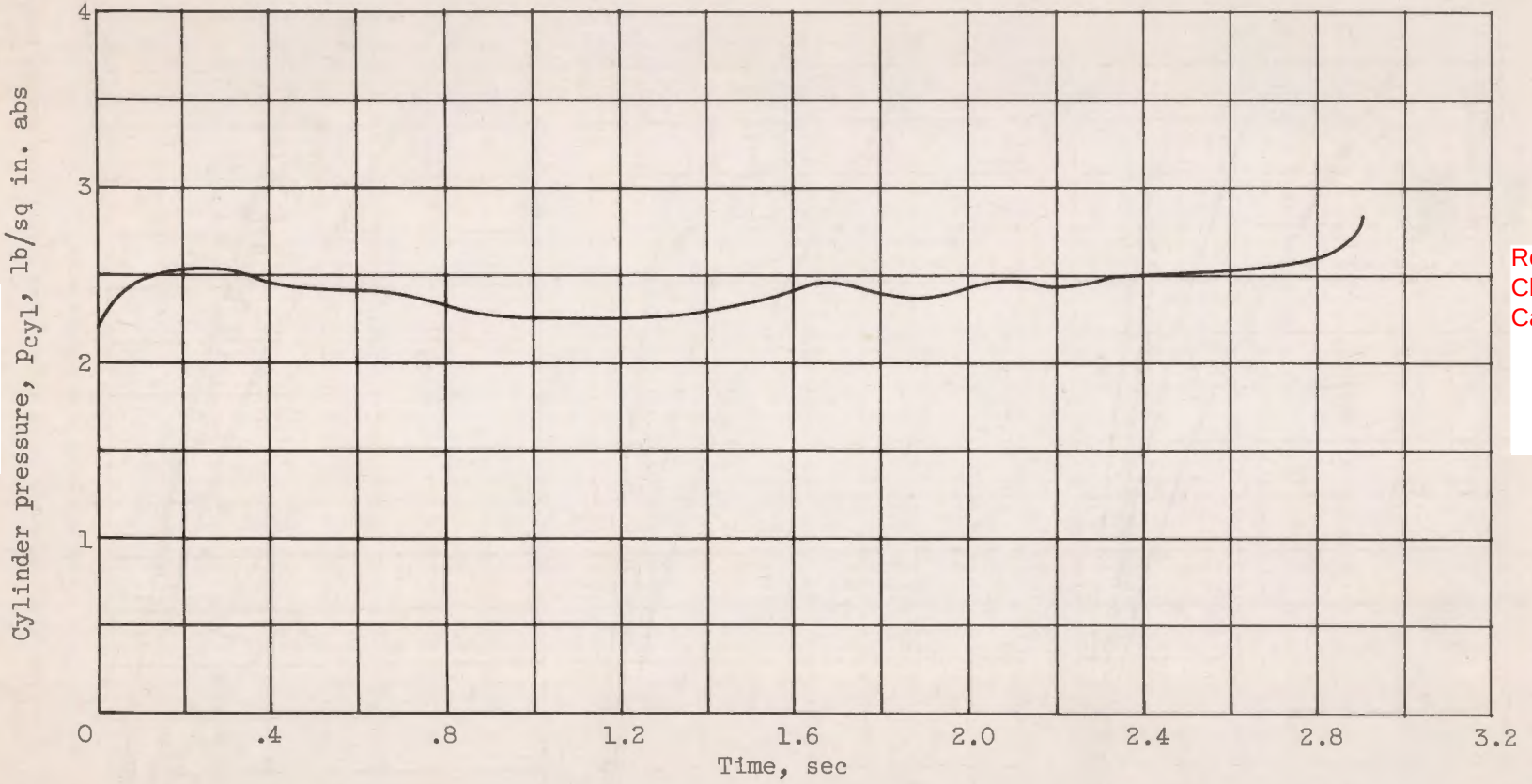

Figure 17. - Time history of cylinder static pressure for model B.

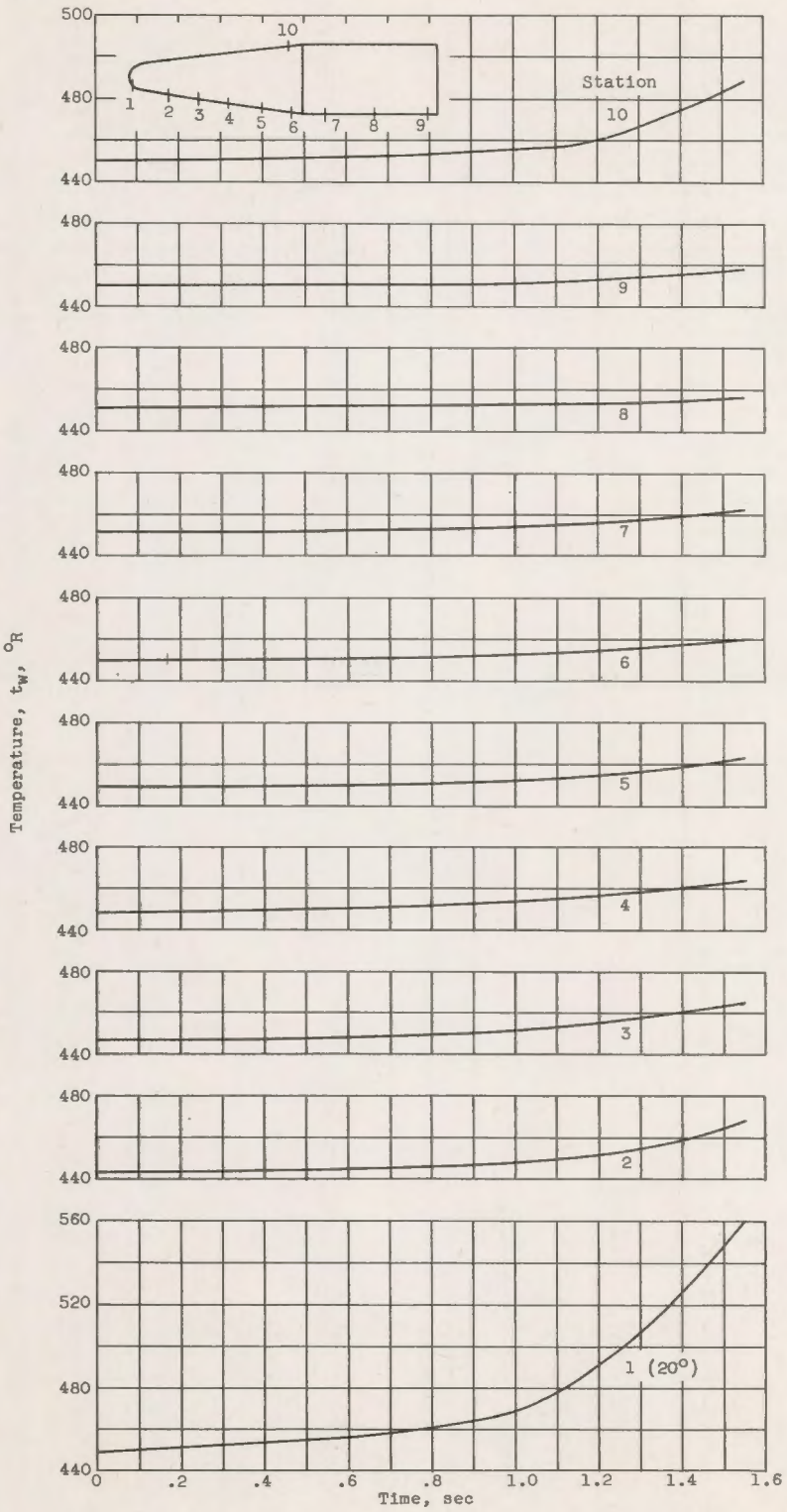

(a) Model A.

Figure 18. - Time history of measured skin temperature.

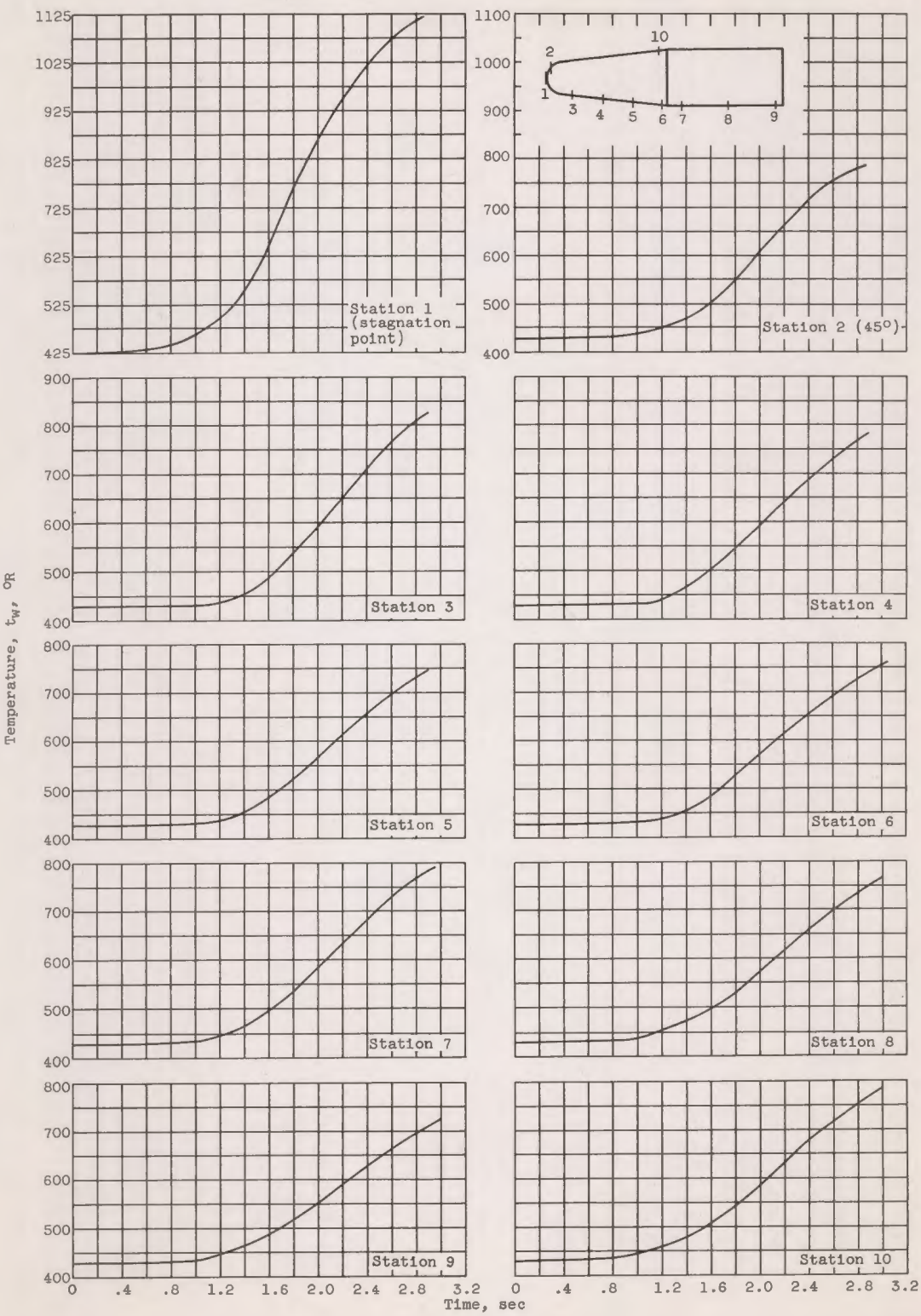

(b) Model B.

Figure 18. - Continued. Time history of measured skin temperatures.

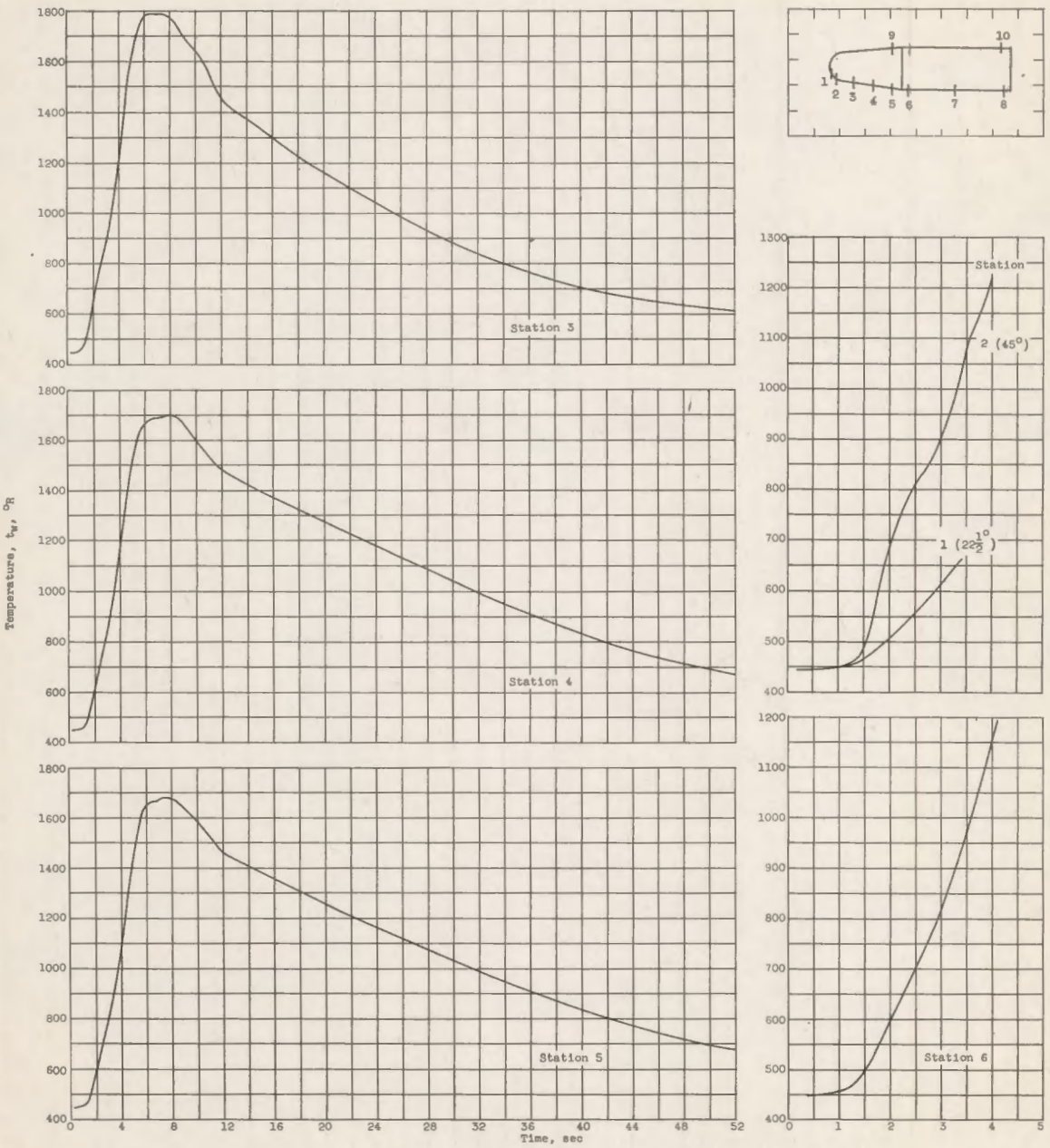

(c) Model C.

Figure 18. - Continued. Time history of measured skin temperatures.

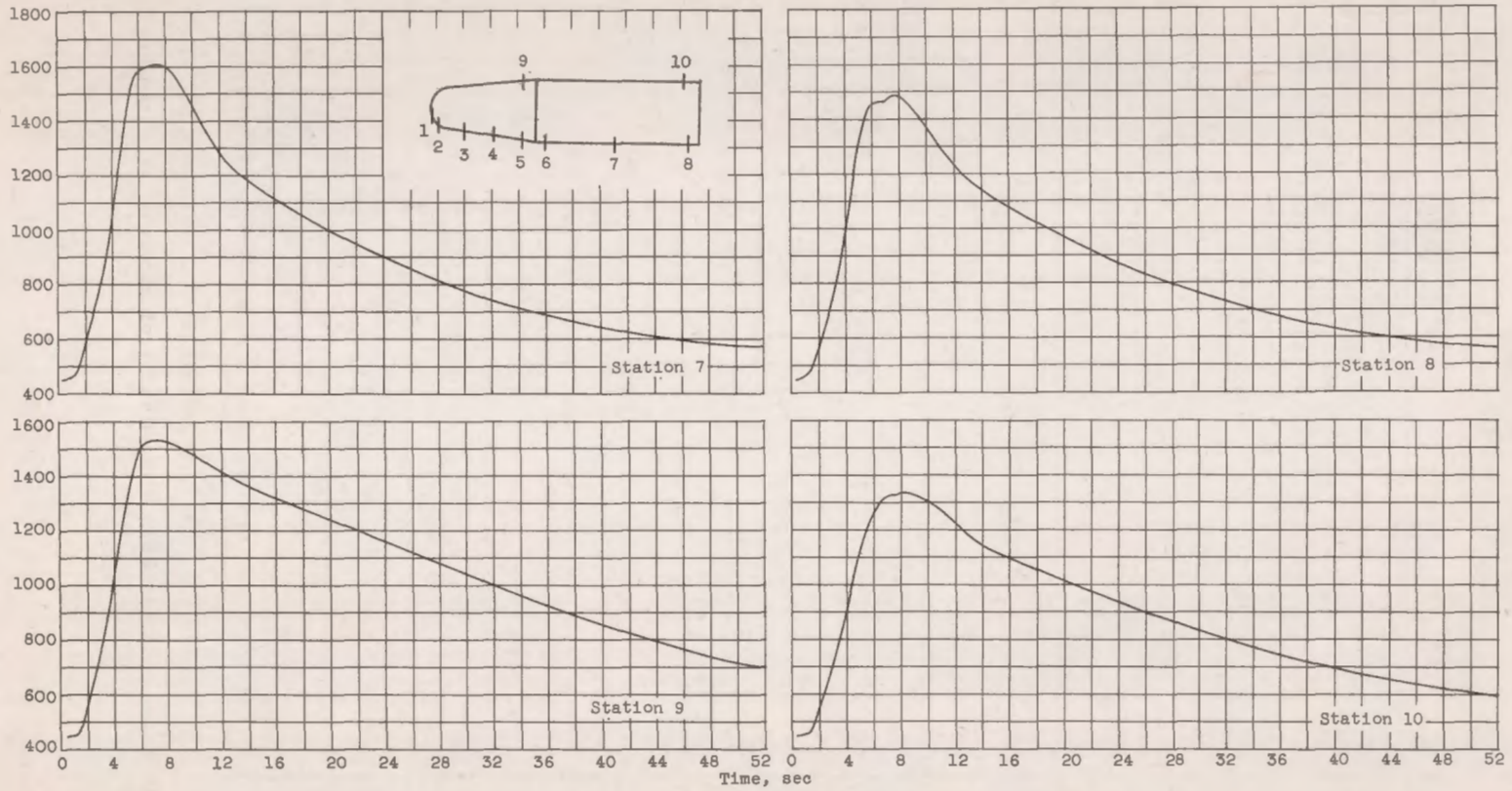

(c) Concluded. Model C.

Figure 18. - Concluded. Time history of measured skin temperatures.

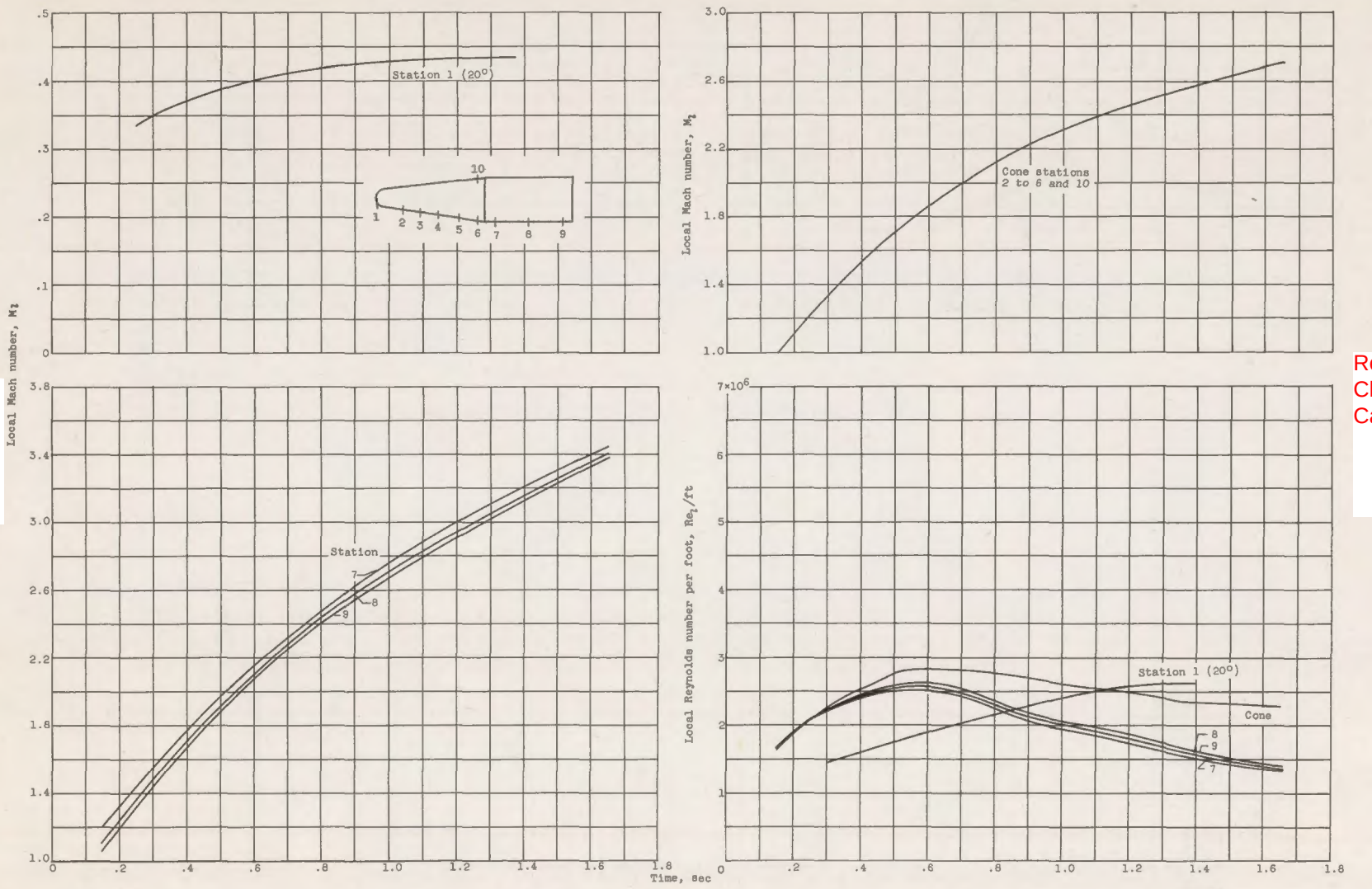

(a) Model A.

Figure 19. - Time history of local Mach number and Reynolds number per foot.

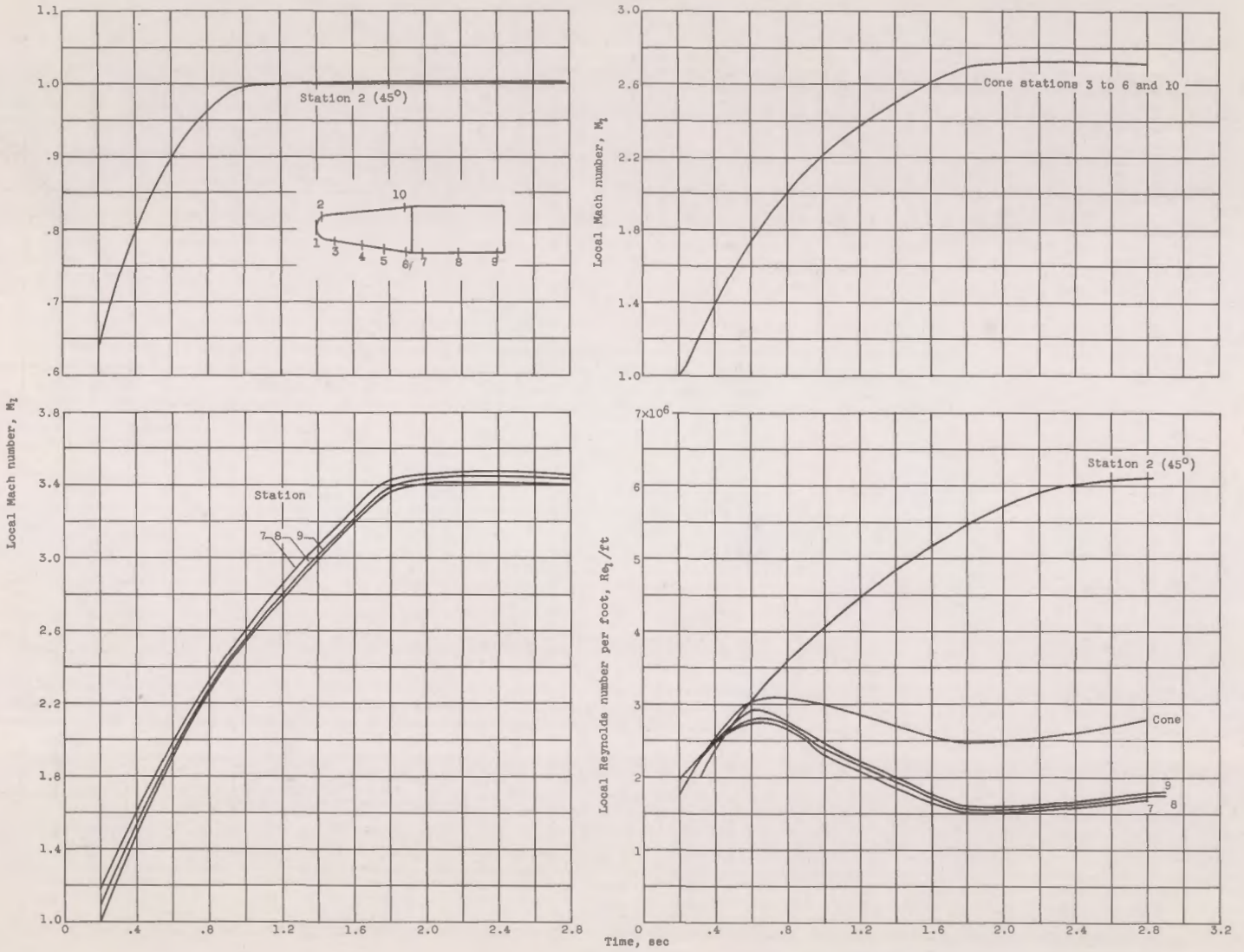

(b) Model B.

Figure 19. - Continued. Time history of local Mach number and local Reynolds number per foot.

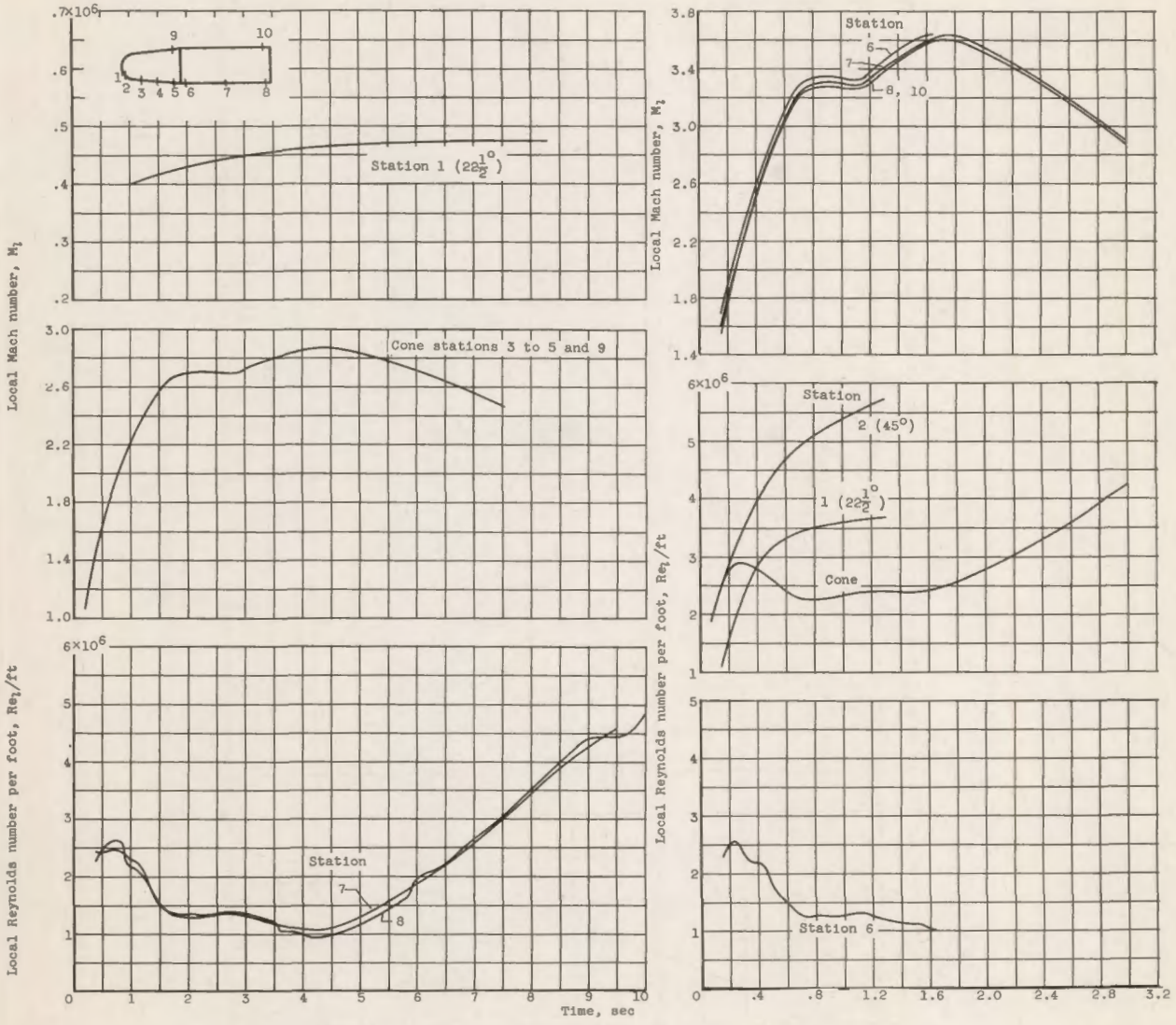

(c) Model C.

Figure 19. - Concluded. Time history of local Mach number and Reynolds number per foot.

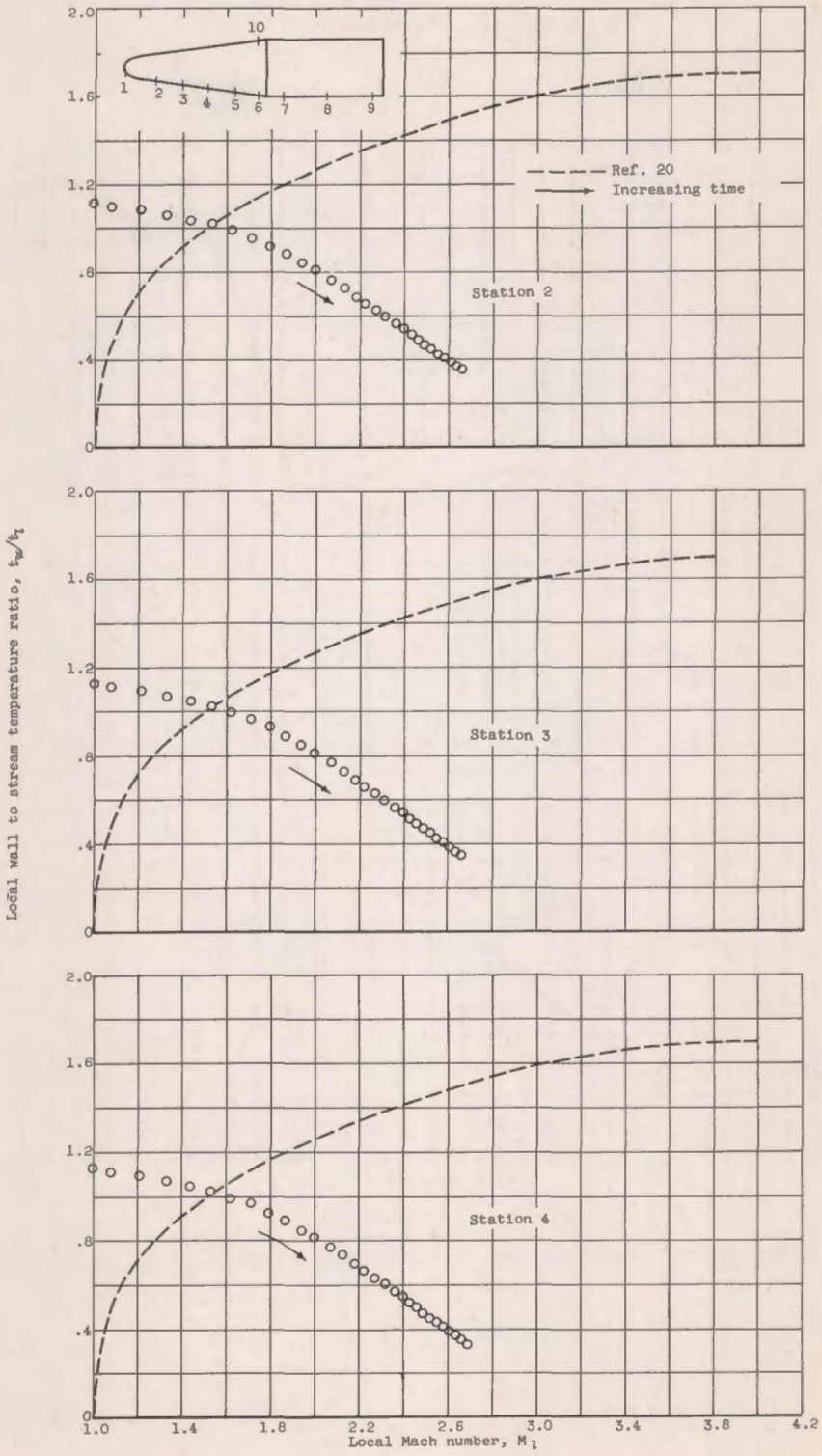

(a) Model A.

Figure 20. - Variations of wall to local stream temperature ratio with local Mach number for the cone and cylinder stations of models A, B, and C.

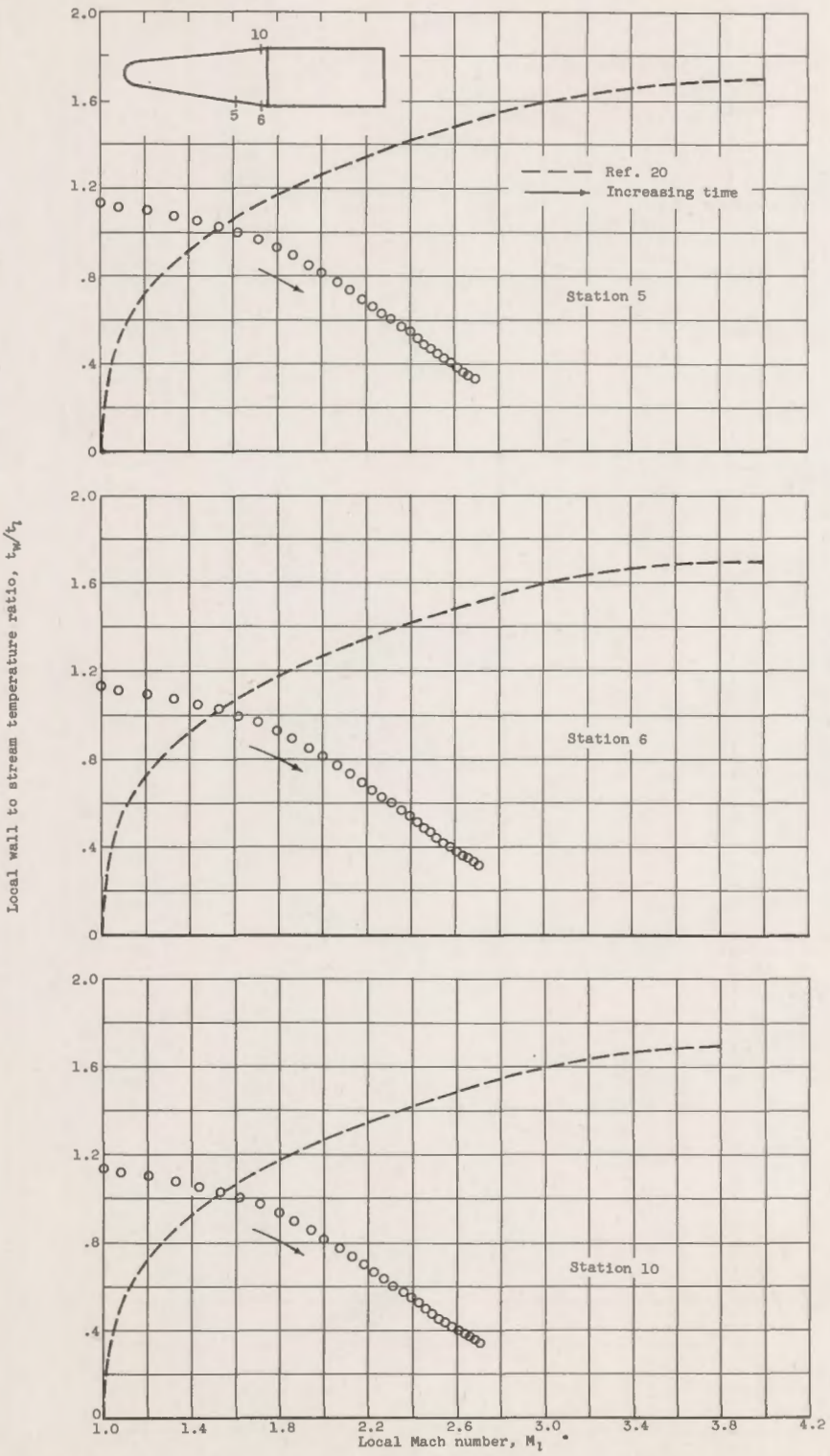

(a) Continued. Model A.

Figure 20. - Continued. Variations of wall to local stream temperature ratio with local Mach number for the cone and cylinder stations of models A, B, and C.

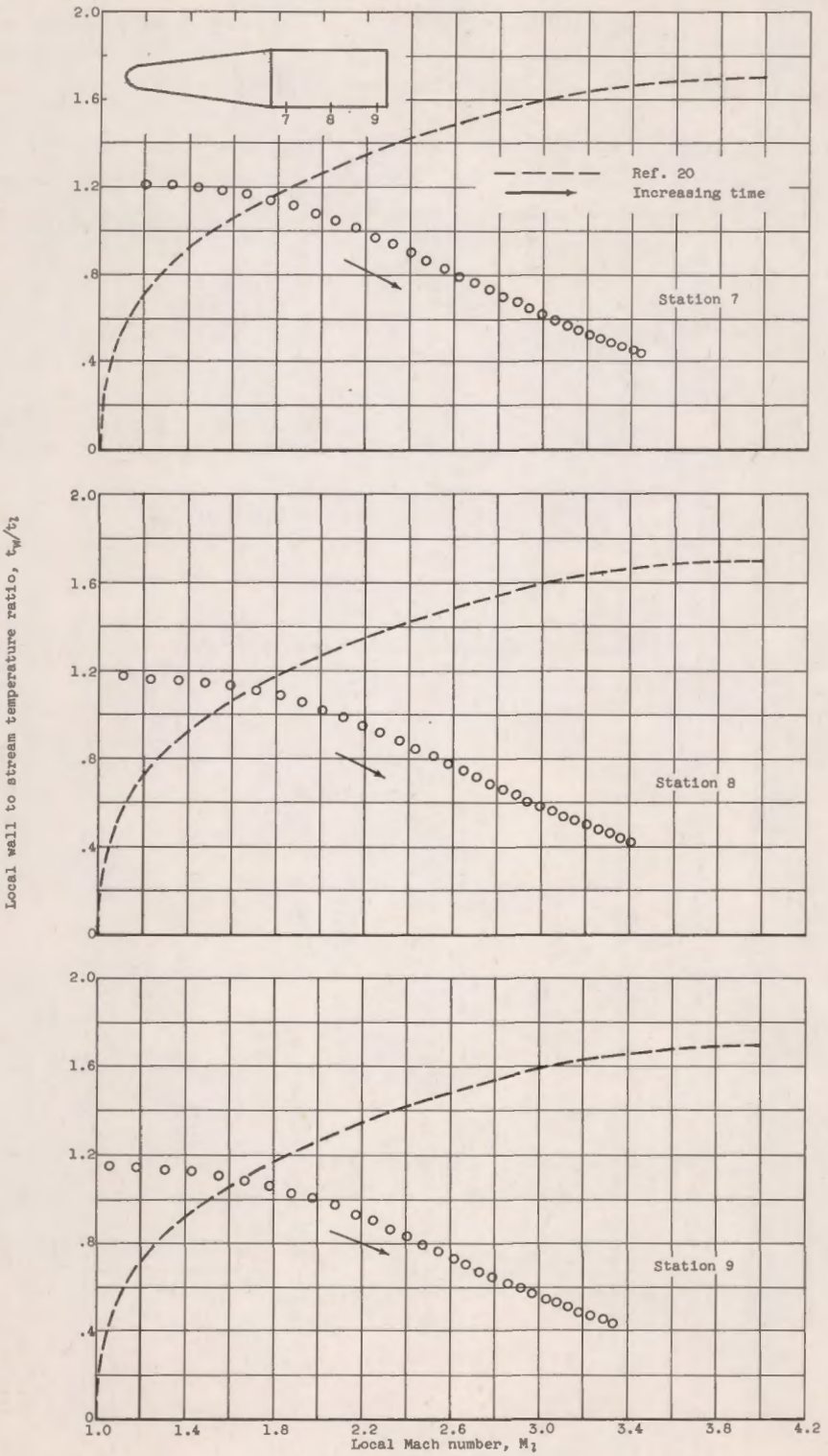

(a) Concluded. Model A.

Figure 20. - Continued. Variations of wall to local stream temperature ratio with local Mach number for the cone and cylinder stations of models A, B, and C.

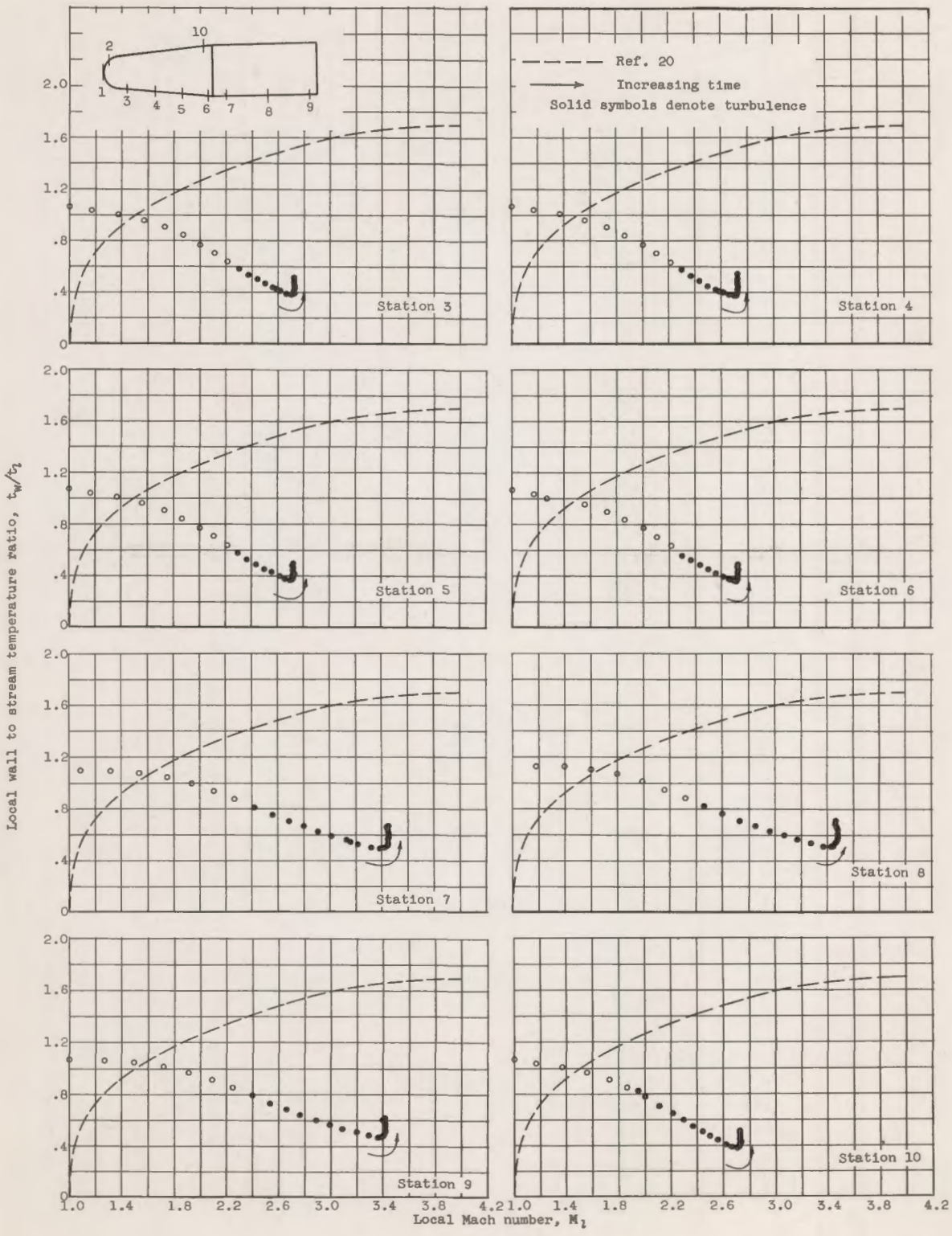

(b) Model B.

Figure 20. - Continued. Variations of wall to local stream temperature ratio with local Mach number for the cone and cylinder stations of models A, B, and C.

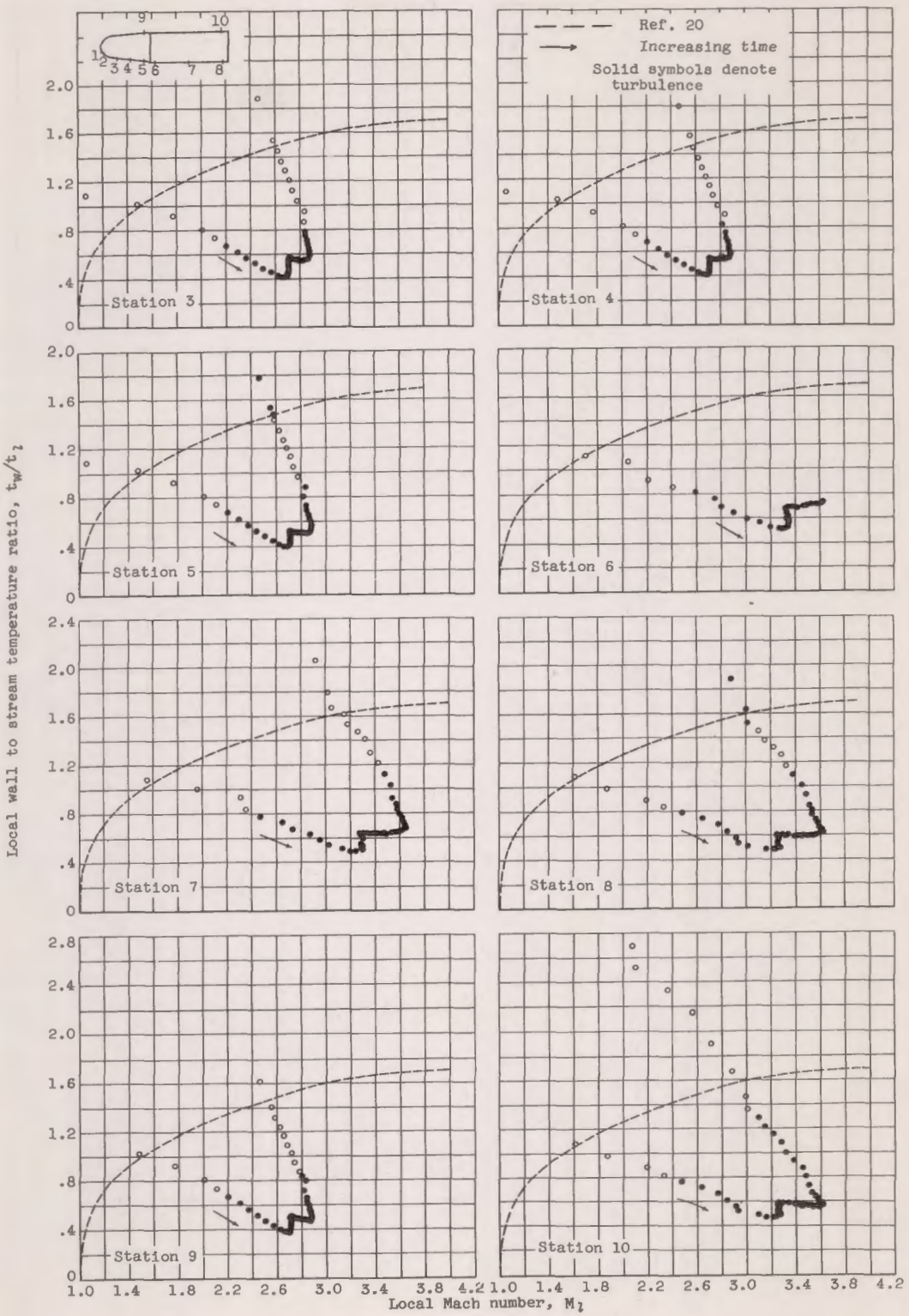

(c) Model C.

Figure 20. - Concluded. Variations of wall to local stream temperature ratio with local Mach number for the cone and cylinder stations of models A, B, and C.